U. S. DEPARTMENT OF COMMERCE
NATIONAL OCEANIC AND ATMOSPHERIC ADMINISTRATION
NATIONAL WEATHER SERVICE
NATIONAL METEOROLOGICAL CENTER

OFFICE NOTE 183

Diagnosis of Numerical Analyses and Forecasts from the Perspective of Quasi-Geostrophic Dynamics

M. Steven Tracton
Development Division

JUNE 1978

1. INTRODUCTION

The conventional statistical measures used by NMC for evaluating numerical analyses and forecasts provide little, if any, insight into the reasons and significance of the end result. Thus, for example, RMS errors and S1 scores convey virtually no information on the type and importance of differences between a forecast and verifying analysis. In contrast, the parameters generated by the oft used Collins and Miller (1975) energy code[1] (e.g., available potential energy) are physically meaningful and readily interpreted. They are extremely valuable, therefore, in diagnosis of such questions as the nature of systematic differences between analyses produced with and without remote sounding data. In that large area and volume averages are considered, however, the energy quantities computed with the Collins and Miller routine can not isolate the effects of individual meteorological features.

Given the limitations of the sort just described, efforts are underway within Systems Evaluation Branch (SEB) to develop "advanced" methods for diagnosing, evaluating, and verifying numerical analysis and forecast systems. One such effort is directed towards application of the diagnostic quasi-geostrophic equations to analyzed and/or forecast height fields. The derived products include the fields of vertical motion and geopotential tendency associated with the principal forcing mechanisms: thermal advection, vorticity advection, and diabatic heating. The influence of surface friction

---

[1]The Collins and Miller code constitutes virtually the only tool currently available at NMC for objectively diagnosing the physical and dynamical behavior of its analysis and forecast systems.

and orography are also determined. In addition, energy budgets and the relative contribution thereto by each forcing function are obtained.

The quasi-geostrophic approach can be used to assess such questions as the significance of differences between analyses produced by differing analysis systems or with differing data sets, the synoptic reasonableness of analyzed and/or initialized fields of divergence, the consistency of forecast fields of vertical velocity with quasi-geostrophic expectations, and the relative and absolute ability of various forecast models to simulate real atmospheric developments. The nature of the derived quantities enables these questions to be addressed in terms which are dynamically meaningful and synoptically familiar. The approach thereby provides useful insights both to the developers and users of NMC's analysis and forecast systems.

The purpose of this Office Note is to describe the quasi-geostrophic approach for evaluating numerical analyses and forecasts and to illustrate its utility via several case studies. The next section (Sec. 2) outlines the basic equations and formulation of the various effects which are considered. Section 3 presents the results of applying the procedures to selected cases. In this section the intent is simply to illustrate the usefulness of the approach, not to present definitive results on any particular question. Finally, Section 4 presents a brief summary of the material contained herein.

2. BASIC EQUATIONS AND FORMULATION OF PHYSICAL PROCESSES

2A. "Omega" equation, etc.

The quasi-geostrophic "Omega" equation may be written

$$\nabla^2 \sigma_0 \omega + f_0^2 \frac{\partial^2 \omega}{\partial p^2} = \overset{(A)}{f_0 \frac{\partial}{\partial p}\left[\vec{V}_g \cdot \nabla(\zeta_g + f)\right]}$$

$$\overset{(B)}{- \nabla^2\left[\vec{V}_g \cdot \nabla \frac{\partial \Phi}{\partial p}\right]}$$

$$\overset{(C)}{- R/c_p p \, \nabla^2 H}$$

where:

Φ = geopotential $\equiv gz$, $\sigma_0 = \frac{\alpha}{\theta}\frac{\partial \theta}{\partial p}$ = static stability $= \sigma(p)$,

$\omega = dp/dt$ (vertical motion),

f_0 = average corolis parameter over region,

H = diabatic heating per unit mass,

$\vec{V}_g = \frac{1}{f_0}\vec{k} \times \nabla \Phi \Rightarrow$ geostrophic velocity, and

$\zeta_g = \frac{1}{f_0}\nabla^2 \Phi \Rightarrow$ geostrophic vorticity.

Terms A, B, and C specify, respectively, the effects of vorticity advection, thermal advection, and diabatic heating upon the field of vertical motion, ω. Rising (sinking) motion occurs in response to an increase (decrease) of cyclonic vorticity advection with height, pronounced warm (cold) advection, and a maximum of diabatic heating (cooling). Further details of the derivation and interpretation of the Omega equation are found in Phillips (1963) and Holton (1972).

Once the field of vertical motion is determined, the geopotential tendency can be obtained directly from the quasi-geostrophic vorticity equation:

$$\nabla^2 \frac{\partial \Phi}{\partial t} = - f_0 \vec{V}_g \cdot \nabla(\zeta_g + f) + f_0^2 \frac{\partial \omega}{\partial p}$$

Note that, since the Omega equation is linear, it can be solved separately for each of the forcing functions (A, B, and C), and the contributions of each to the geopotential tendency determined. That is,

$$\omega_{TOTAL} = \omega_A + \omega_B + \omega_C$$, where

$$\boxed{\nabla^2 \sigma_0 \omega_{A,B\,OR\,C} - f_0^2 \frac{\partial^2 \omega_{A,B,OR\,C}}{\partial p^2}} = \text{A, B or C,}$$

and

$$\frac{\partial \Phi_{TOTAL}}{\partial t} = \frac{\partial \Phi_A}{\partial t} + \frac{\partial \Phi_B}{\partial t} + \frac{\partial \Phi_C}{\partial t},$$ where

$$\frac{\partial \Phi_A}{\partial t} = -f_0 \vec{V}_g \cdot \nabla(\zeta_g + f) + f_0 \frac{\partial \omega_A}{\partial p}$$ and

$$\frac{\partial \Phi_{B\,OR\,C}}{\partial t} = f_0^2 \frac{\partial \omega_{B\,OR\,C}}{\partial p}.$$

In the practical solution of the Omega equation, a three-dimensional grid of data points is employed. The horizontal grid array is a 31x31 square with $\Delta x = \Delta y$ =381 or 191 km (times map factor), depending upon the size and/or area of interest. The vertical grid consists of 10 levels with 100 mb spacing from 1000 to 100 mb. The basic input data are geopotential and relative humidity at mandatory pressure surfaces, interpolated where necessary for conformity with the vertical structure of the grid. The geopotential (i.e., height) fields are sufficient to specify the forcing associated with the vorticity (term A) and thermal (term B) advections, while the relative humidity data supplies the additional information necessary to account for latent heat release (term C) as formulated in Sec. 2B. For convenience, values of the stability factor σ_0 are those of the standard atmosphere. Boundary conditions used in solution of the Omega equation are ω=0 at the lateral walls and p=100 mb. At the lower boundary (p=1000 mb), ω =0 or the frictional and upslope vertical motions are specified (Sec. 2C). All derivatives are

replaced by centered finite differences, and the resulting set of algebraic equations solved by an extrapolated Liebman relaxation scheme. The fields of geopotential tendency are obtained from the derived ω's via relaxation of the vorticity equation for $\partial\Phi/\partial\tau$. Output from the computational procedures consists of ω and $\partial\Phi/\partial\tau$ for an inner 25x25 horizontal array at each 100 mb level.[1]

2B. Latent heat release

The main contribution to H is assumed to be from heat released by condensation, and, of that, only the precipitation associated with stable saturated ascent is considered. The appropriate expression is

$$H = -L\omega \frac{dQ_s}{dp} \Delta S$$

where $\frac{dQ_s}{dp}$ (by assumption) $\approx$ $\frac{\partial Q_s}{\partial p}$ (p, T or thickness)

→ rate of change of saturation specific humidity following the motion,

L = latent heat factor, and

$\Delta S = 1$ if → RH > RH (saturation)
and → $\omega_A + \omega_B < 0$
and → standard height(p) > terrain[2].

$\Delta S = 0$ otherwise.

Substitution of the expression for H into term C of the complete Omega equation yields

---

[1]The $\partial\omega/\partial p$'s at 1000 and 100 mb necessary for solution of the vorticity equation at these levels are obtained by fitting the ω's at bounding levels to a parabolic profile.

[2]Accounts for the effect of variable terrain height on thickness of the precipitating column.

$$\nabla^2 \sigma_m \omega_{total} + f_0^2 \frac{\partial^2 \omega_{total}}{\partial p^2} = A + B, \text{ where}$$

$$\sigma_m = \sigma_0 - \frac{RL}{c_p p} \frac{\partial Q_s}{\partial p} \Delta S.$$

Note that, since $\sigma_m < \sigma_0$ [1], inclusion of latent heat release is formally identical to reduction of the "effective" stability where saturated air is rising. Consequently, the vertical motions associated with the vorticity and thermal advections are enhanced in regions of large-scale precipitation. The component of the total vertical motion due to latent heat release alone is simply the difference between the "wet" and dry" ω's, or equivalently,

$$\omega_c = \omega_{total} - (\omega_A + \omega_B).$$

The precipitation rate associated with the total ω can be obtained from the expression

$$P_{recip} = \sum \omega \frac{\partial Q_s}{\partial p} \frac{\Delta p}{g}$$

where the summation is over the layer 950-350 mb.

2C. Surface boundary effects

The vertical velocity at the top of the surface boundary layer, taken as 1000 mb, results from terrain variations and surface drag. The relevant formulations are, for terrain,

$$\omega_{terr} = \rho_0 g \vec{V}_{1000} \cdot \nabla Z_s$$

and, for friction,

$$\omega_{fric} = -\frac{g \rho_0}{f} \vec{k} \cdot \nabla \times C_d |\vec{V}_{1000}| \vec{V}_{1000},$$

[1]To preserve computational stability, σ_m is set to a value $.1\sigma_0$ if σ_m δ otherwise.

where ρ_0 = standard atmosphere 1000 mb density

Z_s = terrain height

C_d = spatially varying Cressman drag coefficient

In preliminary computations it was found that use of $\vec{V}_{g_{1000}}$ in the above expressions produced unsatisfactory results. Consequently, $\vec{V}_{1000}$ is obtained by adjusting the geostrophic values to account empirically for the less than geostrophic speeds and deflection towards lower pressure characteristic of surface flow. The reduction in wind speed varies from 35% over oceans to 55% over mountainous terrain, while the corresponding angle of deflection ranges from 25° to 45°. These values are consistent with the empirical results presented in Petterssen (1956) and Haltiner and Martin (1957). Variations in both cases are linear with the surface roughness, as specified by C_d.

Note that the vertical distribution of ω associated with friction and orography can be obtained as the difference between the total ω with and without inclusion of these boundary effects or via solution of the Omega equation with the forcing functions set to zero and lower boundary conditions specified. The later approach has been adopted.

2D. Energetics[1]

The integrated form of the quasi-geostrophic equation for kinetic energy may be written

$$\overset{(1)}{\frac{\partial K_g}{\partial t}} = \overset{(2)}{-\frac{1}{g}\iint \omega V_{gm} K_g \delta L \delta P} \; \overset{(3)}{-\frac{1}{g}\iint \vec{V} \cdot \nabla \Phi \delta A \delta P} ,$$

where $K_g = (u_g^2 + v_g^2)$ ⇒ kinetic energy of geostrophic motion

[1]See Wiin-Nielsen (1964) for detailed derivations, etc.

$K_g = \frac{1}{g}\iint k_g \delta A \delta p$ ⇒ kinetic energy content of volume having an area A and bounded in the vertical by constant pressure surfaces,

V_{gm} ⇒ normal component of V_g at the boundary, L , and

$\vec{V}' = \vec{V} - \vec{V}_g$ ⇒ geostrophic departure.

According to the above, the kinetic energy content of a region (1) changes with time in response to the flux of kinetic energy across the lateral boundaries (2) and the generation of kinetic energy by ageostrophic flow across the contours (3). Note that, if the ageostrophic wind is considered purely irrotational,

$$\vec{V}' = \nabla\varphi$$

where the velocity potential, φ , is specified by

$$\nabla^2\varphi = \frac{\partial\omega}{\partial p}.$$

The partitioned ω's can thus be used to determine the separate contributions of each forcing mechanism to the kinetic energy generation.

In addition to each of the terms of the kinetic energy equation, the budget of available potential energy is considered. The governing equation is

$$\overset{(1)}{\frac{\partial(APE)}{\partial t}} = \overset{(2)}{\frac{1}{2g}\oint V_{gm}\frac{\alpha'^2}{\sigma_0}\delta L\delta p} + \overset{(3)}{\frac{1}{g}\iint \alpha'\omega'\delta A\delta p}$$
$$+ \overset{(4)}{\frac{R}{c_p g}\iint \frac{\alpha' H'}{\sigma_0}\delta A\delta p},$$

where $\alpha = 1/\rho$, $(\ )'$ = departure from areal average,

and $APE = \frac{1}{2g}\iint \frac{\alpha'^2}{\sigma_0}\delta A\delta p$ = available potential energy content of the region.

From this expression one can see that time changes of the "local" available potential energy (1) result from a flux of that quantity through the lateral boundaries (2), in situ conversions between kinetic and available potential

energies (3) and generation by diabatic heating (4). Note that the seperate effects of each forcing mechanism upon the conversion term can be determined from the relevant components of ω.

In the computer routines, energetic quantities can be obtained for any sub-area of the output 25x25 array, so that attention can be focused upon individual synoptic features. In addition, the sub-area can move with the system in question, thus enabling consideration of energy budgets within a quasi-Lagrangian framework.

3. APPLICATIONS

The purpose of this section is to illustrate some applications of the concepts and procedures just described. The intent here is not to present a definitive evaluation of any given question, but rather to highlight the utility of the approach.

In the first case (Sec. 3.1), the dynamic implications of differences between the operational (HUFF) and LFM (Cressman) analyses for 1200 GMT 22 February 1978 are explored. Section 3.2 examines the relative and absolute merits of differing forecast models in predicting the major cyclogenesis over the U.S., 9-11 January 1975. This case has been discussed by Phillips (1978) within the same context but from a different viewpoint. Section 3.3 examines the influence of latent heat release upon the 9-11 January 1975 storm. The next section (Sec. 3.4) compares the fields of vertical velocity predicted by the 7-layer PE from 0000 GMT 22 February 1978 with the quasi-geostrophic omega's derived from the corresponding forecast height fields. Finally, Sec. 3.5 assesses the significance of differences between the operational and LFM surface analyses, 0000 GMT 23 January 1978, particularly as those differences relate to the effects of surface friction.

3.1 Operational (HUFF) and LFM (Cressman) analysis differences, 1200 GMT 22 February 1978

Figure 1 presents the operational and LFM 500 mb height/vorticity and 1000 mb height/1000-500 thickness charts valid 1200 GMT 22 February 1978. Of interest are the analysis differences relating to definition of the 500 mb trough over the eastern U.S. In the operational version a single vorticity maximum appears over South Carolina. In the LFM, the vorticity pattern is considerably more complex, with distinct maxima appearing east of Cape Hatteras, and over Georgia and Ohio. In addition, a well defined minimum is apparent over northern Virginia. Some differences also exist between the corresponding 1000 mb analyses. The surface low east of Hatteras, for example, is approximately 10 m deeper and 300 km further to the northeast in the operational version.

The following discussion explores the dynamic implications of the operational/LFM analysis differences. No consideration is given to the source of the disparity between analyses, though clearly this is an important question which ultimately must be addressed.

Qualitatively, one can infer differences between the operational and LFM fields of quasi-geostrophic vertical velocity and geopotential tendency from the composite 1000 mb and 1000-500 mb thickness charts shown in Fig. 1 and the composite 500 mb height and geostrophic vorticity analyses displayed in Fig. 2. Thus, for example, while the pattern of vorticity advection in the LFM analysis implies strong upward motion and accompanying 1000 mb height falls over the surface low, the operational analysis suggests that vorticity advection has relatively little effect over the low center.

Quantitatively, detailed differences in the shape, orientation, and intensity of the quasi-geostrophic fields derived from the operational and LFM analyses can be gleaned from visual inspection of Figs. 3 to 9.[1] Shown in these figures are the separate contributions of vorticity (Figs. 3 and 6) and thermal (Figs. 4 and 7) advections to the fields of 700 mb vertical velocity (cm sec^{-1}) and 1000 mb tendency (converted to sea-level pressure tendency in mb hr^{-1}). The combined influence of these forcing mechanisms on the same fields (Figs. 5 and 8) and, in addition, on the 500 mb geopotential tendency (Fig. 9) does not include the effects of surface friction and orography, and the influence of latent heat release has not been considered in this case.

Overall, it is clear from the figures that differences between operational and LFM analyses translate to significant differences in the diagnostically computed quantities and, therefore, in the implied motion and development of the relevant weather systems. Thus, for example, the total (vorticity plus thermal advection) sea-level pressure (SLP) tendencies (Fig. 5), which reflect the fields of low-level divergence associated with the vertical motions, indicate that the surface low east of Cape Hatteras is deepening 1.0 and 0.5 mb hr^{-1} in the LFM and operational analyses, respectively. Moreover, the considerably stronger gradient of SLP tendency across the low in the LFM SLP tendency field implies that the storm is moving towards the northeast much faster in the LFM than in the operational analysis.[2]

---

[1]Computations were performed over the area shown on a subset of the LFM grid after interpolation, in the case of the operational, from the 65x65.

[2]According to Petterssen's (1956) kinematic formulae, phase speed is directly proportional to the gradient of tendency across a low (or trough) and inversely proportional to the intensity of the system. In this case the former effect dominates.

It turns out that the LFM's greater deepening rate and phase speed are more consistent with trends defined by NMC's manually analyzed surface charts. The important point, though, is not that the LFM appears better, but that considerations of this sort address that question independently of the much costlier and possibly less definitive approach of running forecasts from both sets of analyses with the same prediciion model.

Inspection of Figs. 3 to 5 reveals that, by and large, differences in the total SLP tendency result from the vorticity advection term. In that regard, the most obvious difference is that, while the LFM center of SLP falls due to vorticity advection encompasses the surface low, the comparable fall center in the operational tendency field lies to the southwest. This simply reflects in a dynamically meaningful way difference in the slope of the weather system, as defined by the respective locations of the surface low and associated 500 mb short wave in the operational and LFM analyses (Figs. 1 and 2).

Further insights can be obtained by examining the relative contributions of thermal and vorticity advection to the total 700 mb vertical velocity (Figs. 6 to 8). Suffice it to say here that, as expected, each effect relates directly to the previously described differences in SLP tendency.

Of particular interest with regard to the total vertical velocities is that the LFM field is notably more consistent with the cloud distribution observed by the GOES satellite (not shown, won't xerox). Specifically, the marked westward extension of upward motion into Virginia and North Carolina and intense subsidence centered appriximately at 75°W, 30°N in the LFM (Fig. 8) are in much better agreement with the vertical motions implied by the cloud imagery than the corresponding area of ascent and descent in the operational. The key point here again, though, is not that the LFM analysis appears superior,

but that the approach being described is a viable and potentially quite profitable means of addressing that question.

The most pronounced difference between analyses in terms of the total 500 mb height tendencies (which by and large reflect the influence of vorticity advection) relates to the location and orientation of the height fall center east of Hatteras (Fig. 9). The magnitude of the negative tendencies is approximately the same in the two analyses (≈ 25 m hr^{-1}), but the operational height-fall center lies more than 300 km to the southwest of the LFM position. Note too the westward bulge of height falls in the LFM which is not present in the operational. With reference to the 500 mb analyses (Fig. 2), one can see the net effect is that negative tendencies extend through the trough axis in the LFM but not (or, at least, only marginally so) in the operational. The diagnostically computed quantities, therefore, suggest an amplifying upper-level system in the LFM analyses, but one changing little in intensity in the operational version. Subsequent developments tend to confirm the trend implied by the LFM.

The results of the energy computations for this case are summarized in Table 1. Calculations are for the sub-area shown in Fig. 1d which is centered approximately at the location of the surface low off the east coast. Values of the energy parameters thus apply to the structure and developmental potential of this particular weather system. Note that the energy parameters listed pertain to the vertically integrated values for the layers 1000-600 mb (Lower, L), 600-200 mb (Upper, U) and 1000-200 mb (Total, T).

Among the most notable results emerging from Table 1 are i) the kinetic energy (KE) and available potential energy (APE) contents of the region are about the same in the LFM and operational analyses, (ii) the boundary

Table 1. Quasi-geostrophic energetics for operational and LFM analyses, 1200 GMT 22 February 1978. Values are vertically integrated through the layers 1000-600 mb (Lower, L), 600-200 mb (Upper, U), and 1000-200 mb (Total, T).

	OPN	LFM
KE Content		
L	$7.5 \times 10^5 Jm^{-2}$	$7.8 \times 10^5 Jm^{-2}$
U	67.5×10^5 "	62.3×10^5 "
T	75.0×10^5 "	70.1×10^5 "
KE Bound flux		
L	$-3.2\ wm^{-2}$	$0.6\ wm^{-2}$
U	87.1 "	71.5 "
T	84.8 "	72.1 "
APE Content		
L	$11.8 \times 10^5 Jm^{-2}$	$11.9 \times 10^5 Jm^{-2}$
U	8.7×10^5 "	8.8×10^5 "
T	20.5×10^5 "	20.7×10^5 "
KE Generation		
L	$4.6\ wm^{-2}$	$12.4\ wm^{-2}$
U	70.0 "	66.1 "
T	74.6 "	78.5 "
APE Generation		
L	$-0.7\ wm^{-2}$	$3.8\ wm^{-2}$
U	-9.4 "	-2.5 "
T	-10.1 "	1.3 "

flux of KE in the total vertical integral is some 18% greater in the operational, and this mostly reflects differences in the upper layer, iii) at low levels, largely as a result of differences in the effects of vorticity advection (not shown), the generation of kinetic energy is almost three times as large in the LFM analysis, and iv) while in the vertical integral the LFM analysis implies conversion of APE to KE, the reverse process is occurring nearly an order of magnitude faster in the operational analysis.

Overall, the energetics provide a convenient overview of the nature of the analysis differences, and from this perspective the differences appear quite significant. More detailed interpretation of the energetics is possible and clearly desirable, but beyond the scope of this document.

3.2 Intermodel comparison of forecasts from 1200 GMT 9 January 1975

In conjunction with efforts to assess forecast improvement with increased horizontal resolution, predictions were generated from analyses valid 1200 GMT 9 January 1975 with three forecast models and varying grid spacing. Details of this experiment have been reported by Phillips (1978). Therein, Phillips discusses differences between the competing forecasts from the perspective of synoptic judgment and routine statistical parameters. From the perspective of quasi-geostrophic dynamics, this case provides an excellent opportunity to evaluate the performance of differing models and varying horizontal resolutions on a relative (w.r.t. each other) and an absolute (w.r.t. verifying analysis) basis.

Diagnosis of this case, which features major cyclogenesis over the central U.S. and "locked-in'error", is not yet complete. When finished, the evaluation is expected to provide insights into the workings of both real and model atmospheres. For the purposes of this Office Note, comparison of the 24 hour Nested Grid Model (198 km, 45 ^{o}N) and 7-layer P.E. (174 km, 45°N) prognoses will serve to illustrate some of the information available from the diagnostic routines. For this case, quantities were derived on a 31x31 sub-array of the 65x65 grid, though output is displayed only for an inner 13x13 mesh which encompasses most of the U.S. Total here refers to the combined effects of vorticity and thermal advections, surface friction, and orography.[1] Latent heat is not included, but its effect upon observed fields is illustrated in Section 3.3.

Consider first the diagnostically computed quantities derived from the verifying (FINAL) analyses, 1200 GMT 10 January, which are shown in Fig. 10. The field of total SLP tendency (Fig. 11) indicates falls ahead and rises behind the surface low position which exceed 1 mb hr^{-1} in magnitude. At the low center itself the diagnostics indicate a deepening rate of .5 mb hr^{-1}. As shown in Sec. 3.3, the absence of latent heat release in the computations accounts for the difference between this calculated deepening rate and that (1.1 mb hr^{-1}) prescribed by the relevant sequence of surface charts. Vorticity advection, in accord with Sutcliffe (1947) development theory and Petterssen's (1956) forecasting rules, is the principle mechanism (exclusive of latent heat release) contributing to development (-.8 mb hr^{-1}). Thermal advection and orography have no effect on the net deepening rate, but surface frictional effects oppose development at the rate of 0.3 mb hr^{-1}.

---

[1]PE course-mesh terrain.

The 500 mb geopotential tendency field (total) derived from the verifying height analyses is shown in Fig. 12. Negative tendencies lie in advance and positive tendencies to the rear of the 500 mb trough, with the largest height falls and rises corresponding to (approximately) 15 m hr^{-1} and 8 m hr^{-1}, respectively. Note that height falls extend through the trough axis and indicate the trough is deepening at a rate of about 7 m hr^{-1}.

Together, the SLP and 500 mb tendencies suggest an amplifying system translating towards the northeast. Quantitatively, estimates of the phase speeds (using Petterssen's kinematic formulae) of the upper trough and surface low indicate the former is overtaking the latter, consistent with the occulusion process.

In the 24-hour prognoses from 1200 GMT 9 January (Fig 13), both models accurately forecast the depth of the surface low (-80 m ≃ 990 mb), though the NGM predicts the low center to be somewhat closer to the observed position. At 500 mb, NGM and 7-layer forecasts appear very similar, but each places the trough axis somewhat further to the east than the verifying position.

The respective SLP and 500 mb total tendency fields (Fig. 14 and 15) translate NGM and 7-layer forecast height differences into differences between the implied motion and development of this weather system. Among those differences is that, while the 7-layer indicates some deepening (-0.3 mb hr^{-1}) is occurring, the tendency at the surface low center in the NGM is nil (Fig. 14). Both models underestimate the contribution of vorticity advection to surface deepening by approximately 50% (not shown). In addition, while thermal advection has no effect on the deepening rate in the verifying analysis, asymmetries in the field of thermal advection of both models yield +.4 mb hr^{-1} surface pressure rises over the low. Analysis of the predicted thickness patterns suggests this error may reflect deficiences in the models' treatment of the cold air outbreak

in the lee of the Rockies. Further study is required (model terrain, boundary layer formulations, etc.). The principal point to be made here is that the diagnostics suggest a possible avenue of investigation and provide a means of further pursuit of the question.

At 500 mb, the computed tendencies (Fig. 15) indicate that the trough is deepening in both forecasts, but only at about half the rate in the verification. Of possibly more significance, however, is that in each prognosis the tendencies imply a much larger component of motion towards the east than in the verification. In conjunction with the respective SLP tendencies, this suggests dissociation of surface and upper-level systems in the prognoses, consistent with the occurrence of "locked-in'error". Note too that disparities between the motion of surface and 500 mb features implied by the tendencies is somewhat greater in the 7-layer than NGM; and, in fact, as noted by Phillips (1978), the degree of locked-in-error was greater in the 7-layer than NGM. The diagnostic output thus provides an indication of locked-in-error earlier in the forecast runs than might have otherwise been apparent. More importantly, though, complete evaluation of the diagnostics, including the separate effects of the contributing mechanisms, may shed some light on the nature of this perplexing problem.

3.3 Effects of latent heat release

For illustrating the sort of information available from the latent heat computations Figs. 16 to 18 display some of the output diagnosed from the FINAL analysis valid 1200 GMT 10 January 1975. The areal coverage of the derived (large-scale only) precipitation agrees reasonably well (Fig. 16) with the observed distribution. Except for the thunderstorm activity along

the cold front in southern Arkansas and Louisiana, the computed rainfall rates also appear reasonable.[1] The maximum computed rainfall rate is .08 in hr^{-1} just east of the low center.

The latent heat induced 700 mb vertical velocity field (Fig. 17) indicates maximum rising motion somewhat in excess of 6 cm sec^{-1}. The associated maximum in the SLP tendency field (Fig. 18) is .6 mb hr^{-1}. Note that surface pressure falls extend over the low center, so that condensational heating contributes both to motion and development of the surface cyclone. Of the total computed deepening rate (1.0 mb hr^{-1}), latent heat contributes .5 mb hr^{-1}. Though perhaps fortuitous, inclusion of latent heat release effectively accounts for the previously noted (Sec. 3.2) difference between computed and observed (1.1 mb hr^{-1})[2] deepening rates. The calculations thus indicate (in this case) the importance of the release of latent heat to the development process. Presumably, then, each model's ability or inability to predict the evolution of the storm is closely related to the adequacy of the precipitation forecasts. Comparisons of the differing forecast models run on this case should provide further insights into this question.

An interesting aspect of the energetics associated with the condensational heating[3] is that the generation of APE ($\alpha' H'$ term) is less than the conversion of APE to KE ($\omega' \alpha'$ term) (3.1 versus 4.4 w m^{-2}, respectively). That is, unlike Danard's (1966) frequently cited example, in this case the positive contribution of latent heat release to changes in APE is less than the nega-

---

[1]More definitive statements on this must await analysis of the actual instantaneous (i.e., 1 hr) amounts RH(SAT)=85% in these computations.

[2]Vorticity adv: -0.8, thermal adv: 0.0, friction: +0.3, latent heat: -0.5.

[3]Energy computations apply to the entire area shown in Fig. 16.

tive effect arising from the induced vertical motion. Interpretation of this result must await further study of the complete energy budgets of both real and model atmospheres.

Finally, note that the latent heat calculations can be applied to assess not just the differences between verifying analyses and forecasts, but also the differences between two or more analyses. Thus, for example, the significance of HUFF and LFM analysis differences (including relative humidity) can be viewed from the meaningful perspective of differences in the implied instantaneous precipitation rates.

3.4 Forecast versus quasi-geostrophic vertical velocities

It frequently appears that there is less information in the field of vertical velocity explicitly forecast by a given model than that expected from quasi-geostrophic reasoning. That is, there appears to be more (useful) detail in the vertical velocities inferred from the fields of forecast thermal and vorticity advections than in the model's forecast vertical motion. If so, it probably results from the spatial smoothing and time averaging applied to the forecast ω and suggests the possibility of using the derived rather than forecast fields for guidance purposes.

An example of inconsistency between output and derived vertical motions is provided by the 36-hour 7-layer forecast valid 1200 GMT 23 February. Subjectively, the forecast thermal and vorticity advections imply fairly pronounced rising motion over the south-central U.S. (Fig. 19). Objectively, the model explicitly forecasts only an elongated area of ascent (Fig. 20). oriented north-south ahead of the surface and upper troughs. A well defined maximum of rising motion, however, is seen in the field of vertical velocity

derived from the forecast height fields (Fig. 21).[1] The differences here may reflect real ageostrophic effects, result from the aforementioned smoothing and averaging of predicted ω's, or some combination thereof. Examination of many more cases is required before that question can be answered with surety. On the face of it, one has the impression that the diagnosed vertical velocity possesses greater utility in specifying the areas of active weather predicted by the model.

Whatever the actual situation in this case, the above illustrates the potential usefulness of the diagnostic procedures in assessing the consistency between explicit and derived vertical motions and in providing improved guidance products to the field. With regard to the former use a parallel application is to assess initialized fields of vertical motion (i.e., divergence) provided the 7-layer and LFM from earlier forecast runs. Perhaps the vertical velocities diagnosed from the analyzed height fields are more reasonable and, therefore, potentially more helpful to the models. With respect to the later use, a parallel application might be to use such quantities as the derived instantaneous precipitation rates and 500 mb height and/or SLP tendencies as guidance material for interpreting forecast developments. It is felt that these possible applications of the diagnostic routines deserve further appraisal.

3.5 1000 mb HUFF and LFM analysis differences - frictional effect

Not surprisingly, the operational (HUFF) 1000 mb analyses characteristically underspecify the intensity of deep cyclones. The corresponding LFM (Cressman) analyses, on the other hand, more often than not adequately

---

[1]Only the thermal and vorticity advection terms (and lower boundary conditions) are included in these computations. There was no precipitation forecast in the area of interest, so latent heating does not play a role.

reflect the true depth of intense storms. The consequences of such analysis differences, especially upon the surface frictional effect, can be rather large.

To illustrate, consider the major cyclone centered over Southern Quebec, 1200 GMT 26 Jan 1978. The 1000 mb low in this case is 132 m ($\simeq$ 18 mb) deeper in the LFM analysis (Fig. 22) and correctly reflects the available surface observations.

The effect of friction, of course, is to induce upward motion over the low which decreases in magnitude with increasing elevation. The associated low-level divergence produces the surface pressure rises shown in Fig. 23. At the low center, the tendency fields indicate that friction acts to fill the storm at rates of 2.0 and .8 mb hr^{-1} in the LFM and operational analyses, respectively. The first point of note is that the effect of friction is quite powerful, as well it must be, or storms would develop much more intensely than observed. Second, the diagnostics indicate that differences in the analyzed intensity of the system are dynamically signfiicant. Though this case may be an extreme example, the implication of such differences to forecasts should be assessed. The diagnostics can be a useful tool in further investigation.

Finally, it should be noted that the differences in 1000 mb analyses are reflected aloft, so that the diagnostics produce significant differences (e.g., in the 700 mb ω) associated with the thermal and vorticity advection terms.

4. SUMMARY

Efforts are underway within Systems Evaluation Branch to develop improved methods for diagnosing, evaluating, and verifying numerical analysis and forecast systems. The effort described herein consists of applying the diagnostic quasi-geostrophic equations to analyzed and/or forecast height fields. The derived products include the fields of vertical motion and geopotential tendency associated with the primary forcing functions, i.e. thermal advection, vorticity advection, and diabatic heating. The effects of surface friction and terrain are also computed. Additionally, energy budgets and the relative contribution thereto by each forcing mechanism are obtained. The purpose of this Office Note has been to illustrate the utility of the approach outlined via several case studies. As seen, the diagnostic procedures provide valuable insight into such questions as the significance of analysis differences, the consistency between explicitly forecast fields of vertical velocity and those derived quasi-geostrophically from predicted height fields, the relative and absolute importance of latent heat release on surface development, and the ability of various forecast models to simulate real atmospheric developments. The principal message hopefully drawn from discussion of the case studies is that these questions are addressed in terms which are dynamically meaningful and synoptically familiar, and, therefore, the derived quantities provide considerably more information than, for example, computation of RMS differences or S1 scores. Such information should be of value both to developers and users of NMC's analysis and forecast systems.

It should be noted that application of the quasi-geostrophic equations is not the most sophisticated approach possible. Much the same function can be accomplished through use of the diagnostic balance model (Krishnamurti, 1968). Geof DiMego, in fact, is currently working on balance model routines which will provide information similar to that described herein. A principal advantage of using the balance model is that output (e.g. vertical velocities) can be derived from height or wind fields, so that, for example, one can assess the significance of differences between wind as well as height analyses. Another prime advantage is that non-geostrophic terms, such as deformation and divergence, are included in the balance model version of the Omega equation. The principal disadvantage of the balance model (vis-a-vis the quasi-geostrophic approach) is its numerical complexity and concomitant computer requirements. In essence, while the balance model is more theoretically sophisticated, the quasi-geostrophic approach is simpler and faster to run.

In the near future we expect to compare results obtained from application of the quasi-geostrophic and balance models to the same case (9-11 Jan 1975). Given the conceptual differences between the two approaches, it is likely that application of both will yield more information than separate consideration of either.

REFERENCES

Danard, M. B., 1966: On the contribution of released latent heat to changes in available potential energy. J. Appl. Meteor., Vol. 5, pp. 81-84.

Krishnamurti, T. N., 1968: A diagnostic balance model for studies of weather systems. Mon. Wea. Rev., Vol. 96, No. 4, pp. 197-207.

Haltiner, G. and F. Martin, 1957: Dynamical and Physical Meteorology. McGraw-Hill, 454 pp.

Holton, J. R., 1972: An Introduction to Dynamic Meteorology. Academic Press, 319 pp.

Phillips, N. A., 1963: Geostrophic Motion. Reviews of Geophysics, Vol. 1, No. 2, pp 123-176.

Phillips, N. A., 1978: A Test of finer resolution. NMC Office Note 171, NMC, Washington, D.C.

Petterssen, S., 1956: Weather Analysis and Forecasting. McGraw-Hill, 478 pp.

Sutcliffe, R. C., and A. G. Forsdyke, 1950: The theory and use of upper-air thickness patterns in forecasting. Quart. J. Roy. Meteor. Soc., 76, 189-217.

Wiin-Nielsen, A., 1964: On energy conversion calculations. Mon. Wea. Rev., 92, pp. 161-167.

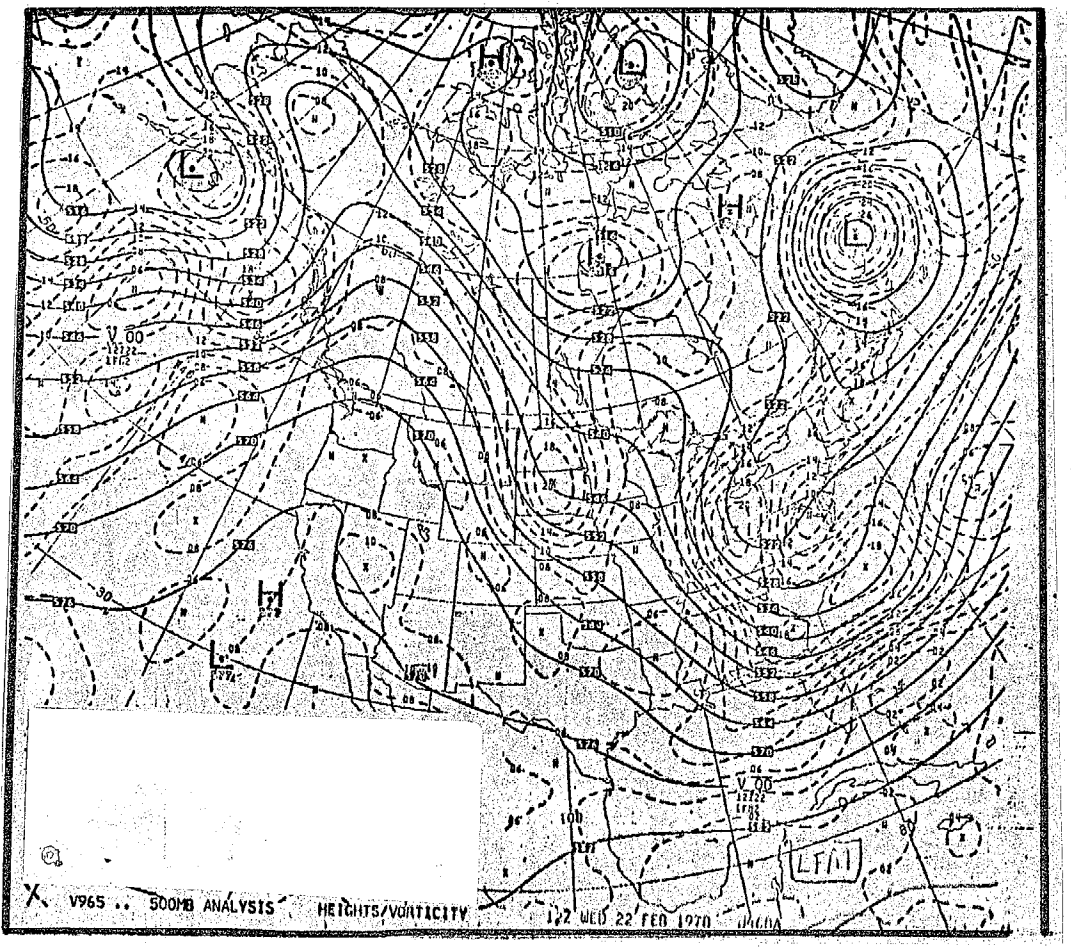

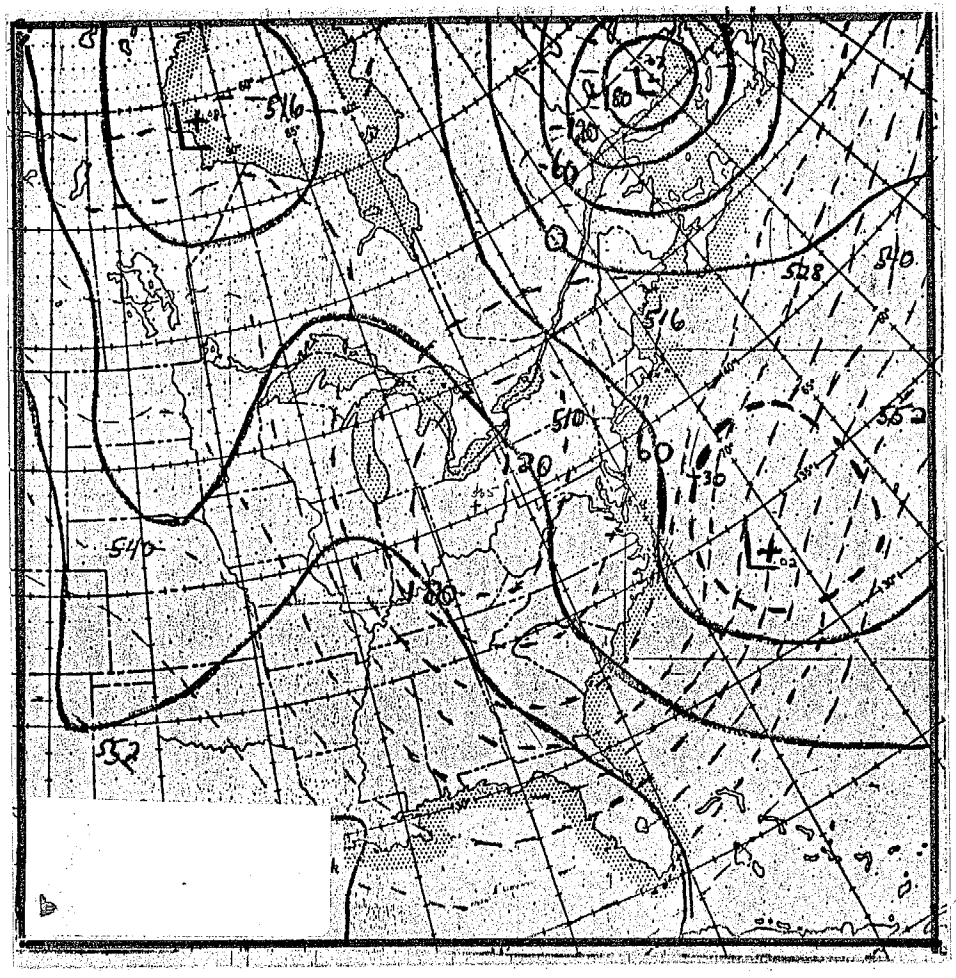

Fig 1a, b

LFM: 500 mb ht/VORT AND 1000 mb ht/1000-500 mb thickness.

1200 22 FEB 1978

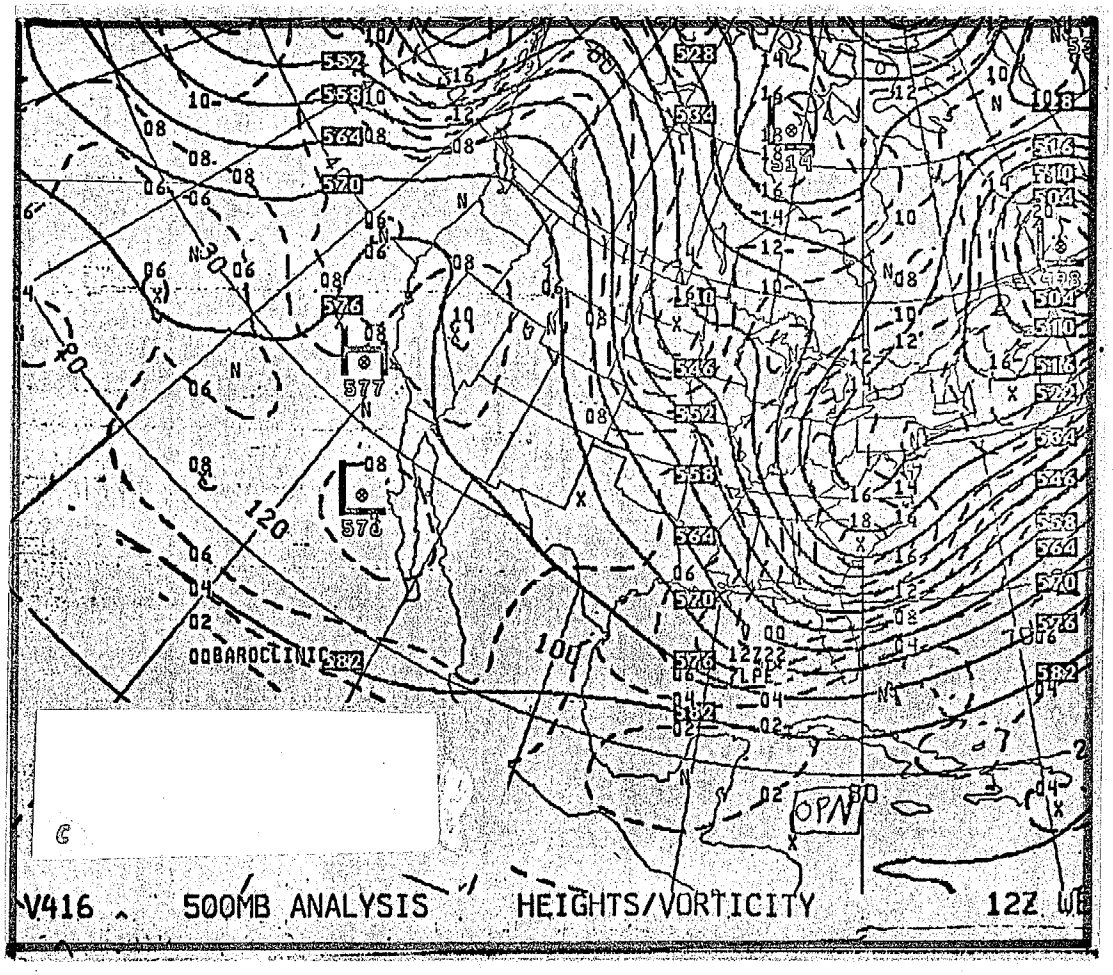

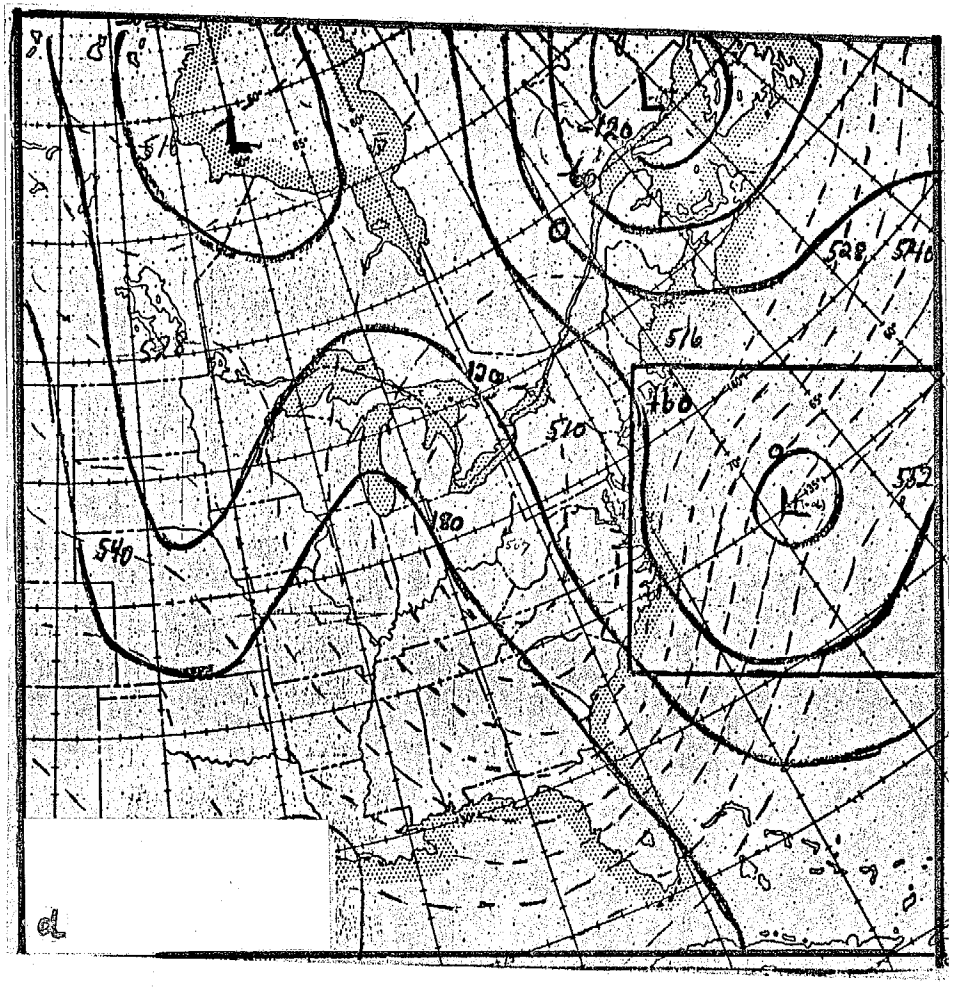

Fig 1c, d

OPN: 500 mb ht/VORT AND
1000 mb ht/1000-500 THICKNESS
(INSCRIBED SQUARE => AREA FOR ENERGY COMPUTATIONS)
1200 22 FEB 1978

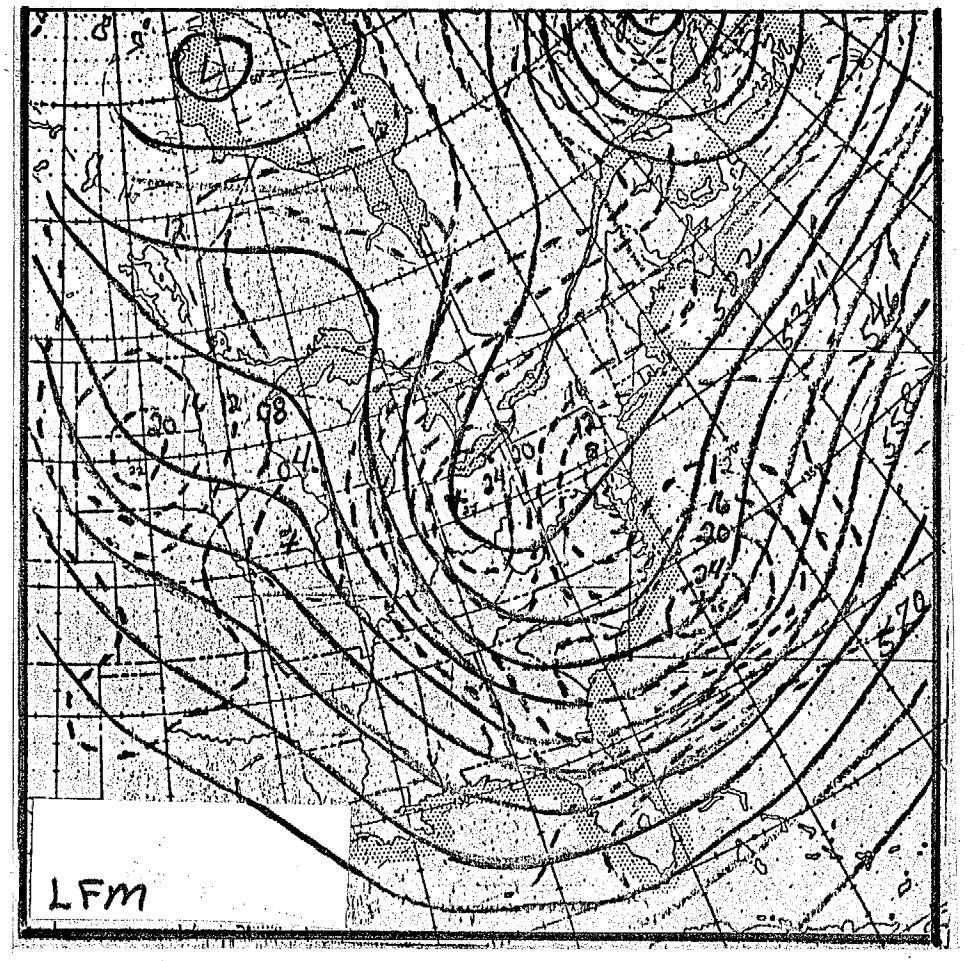

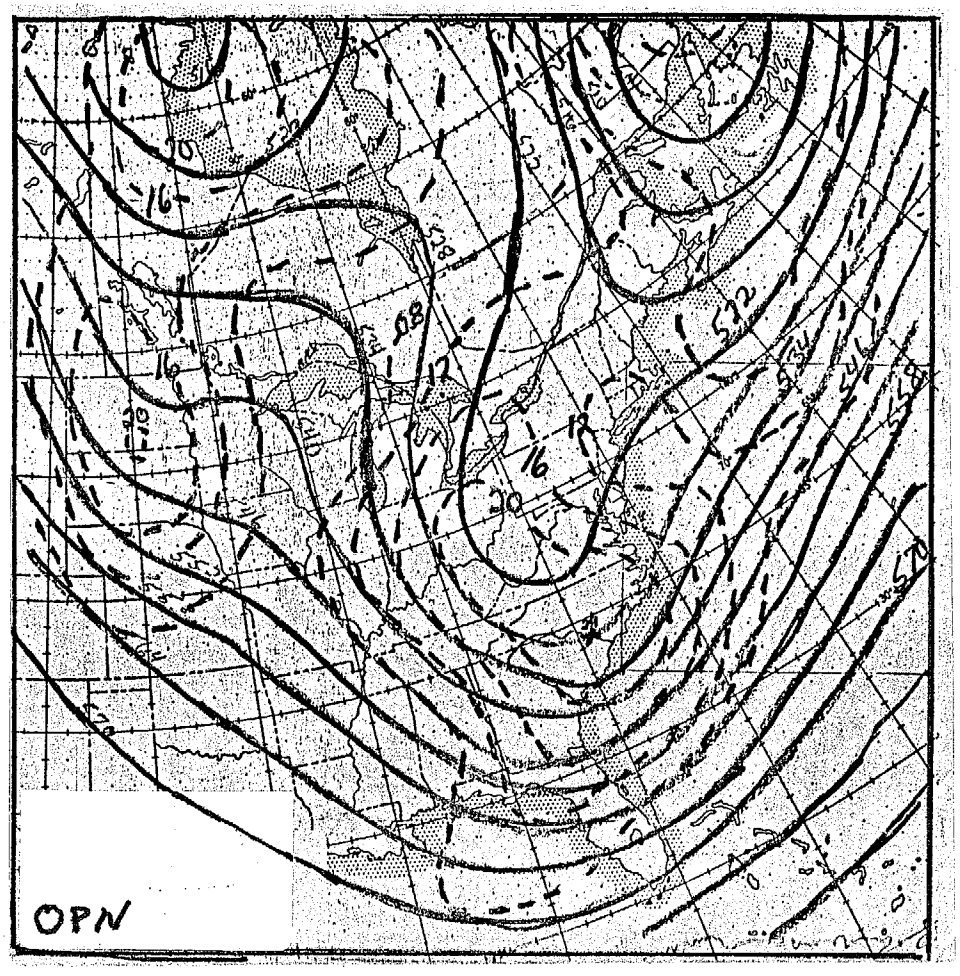

FIG 2.

LFM AND OPN 500MB ht/
GEOSTROPHIC VORT

1200 22 FEB 1978

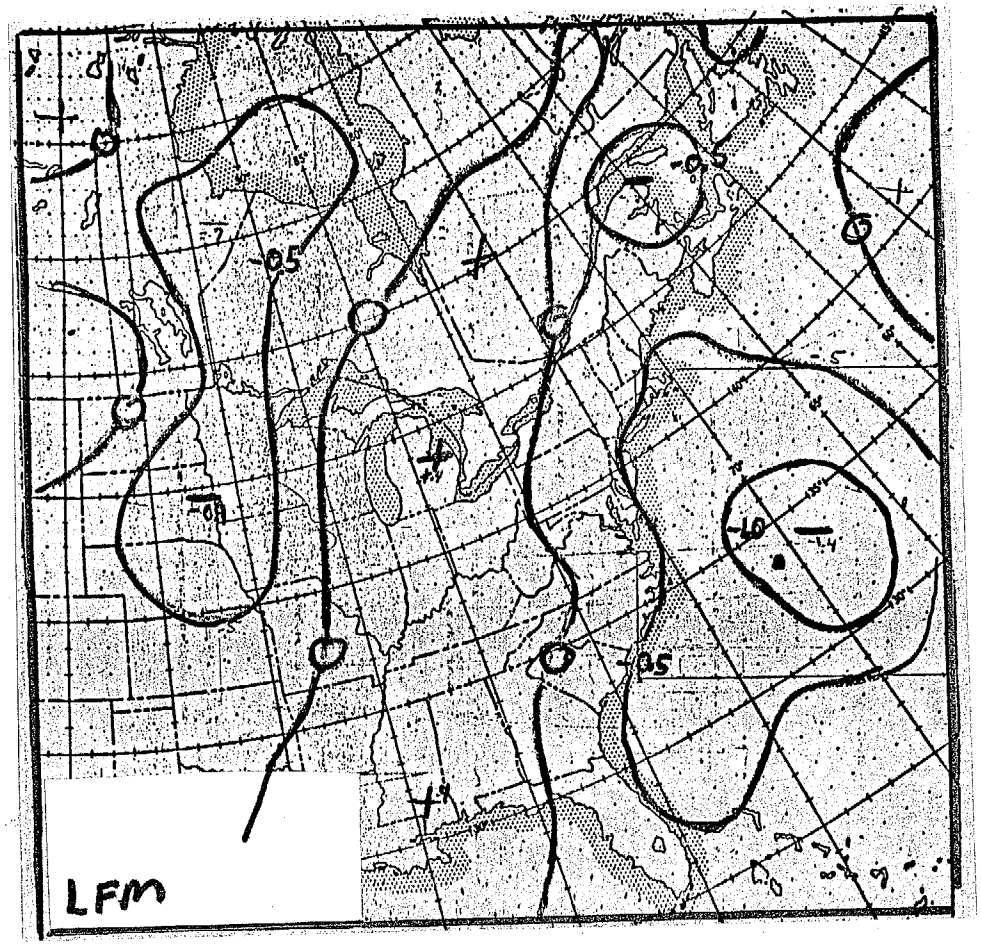

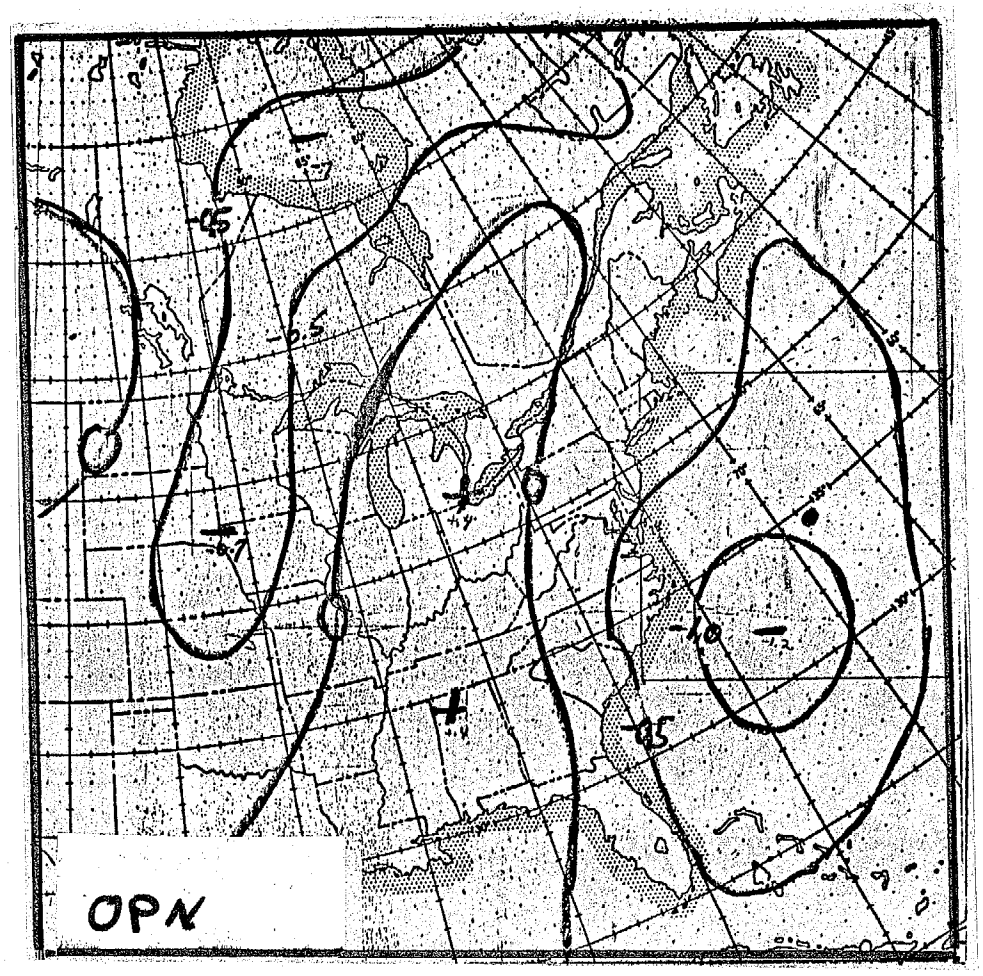

FIG 3.

LFM AND OPN VORT. ADV. SLP TEND. (mb hr⁻¹). ● ⇒ SURFACE LOW CENTER

1200 22 FEB 1978

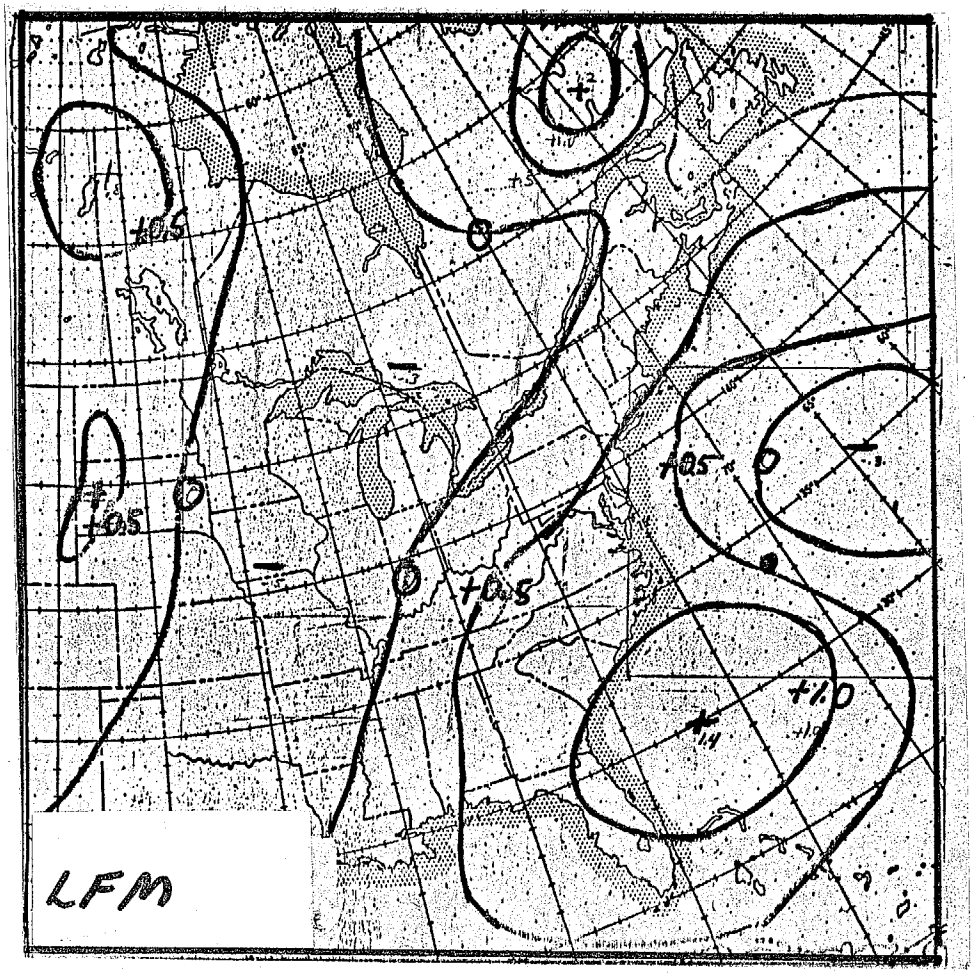

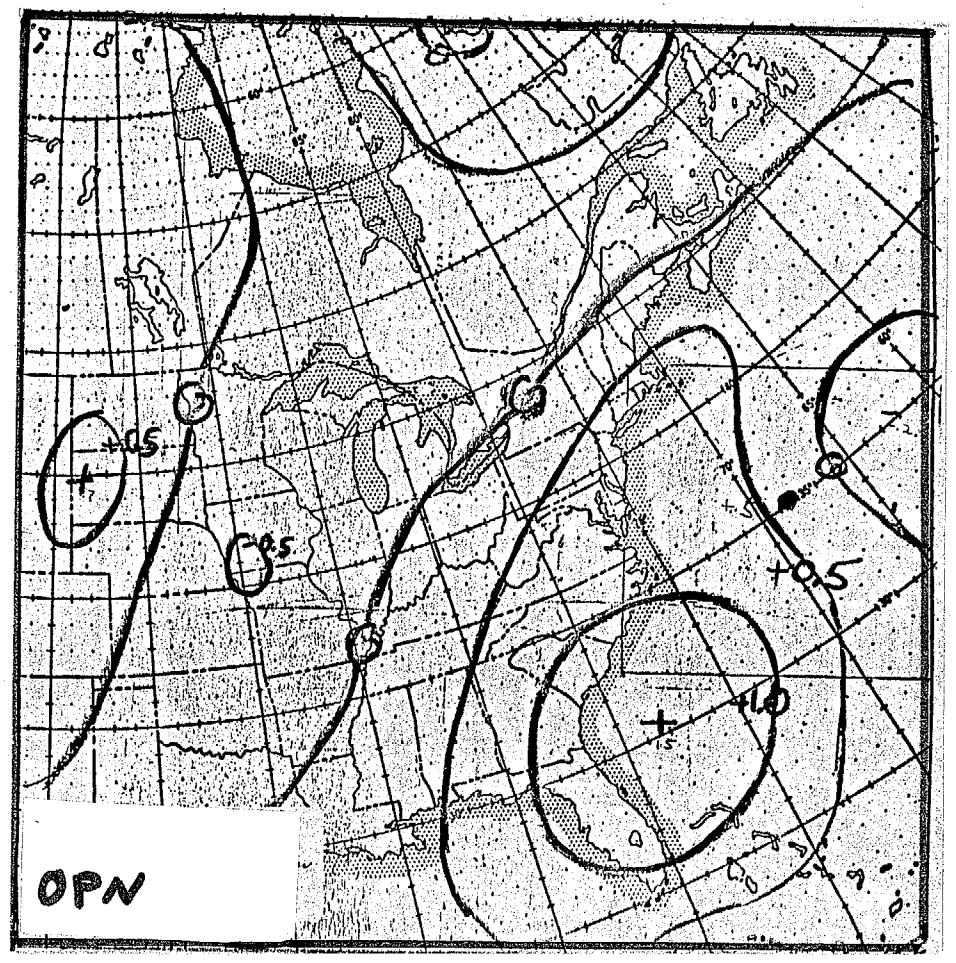

FIG. 4

LFM AND OPN THERMAL ADV. SLP TEND (mb hr⁻¹)

● => SURFACE LOW POSITION

1200 22 FEB 1978

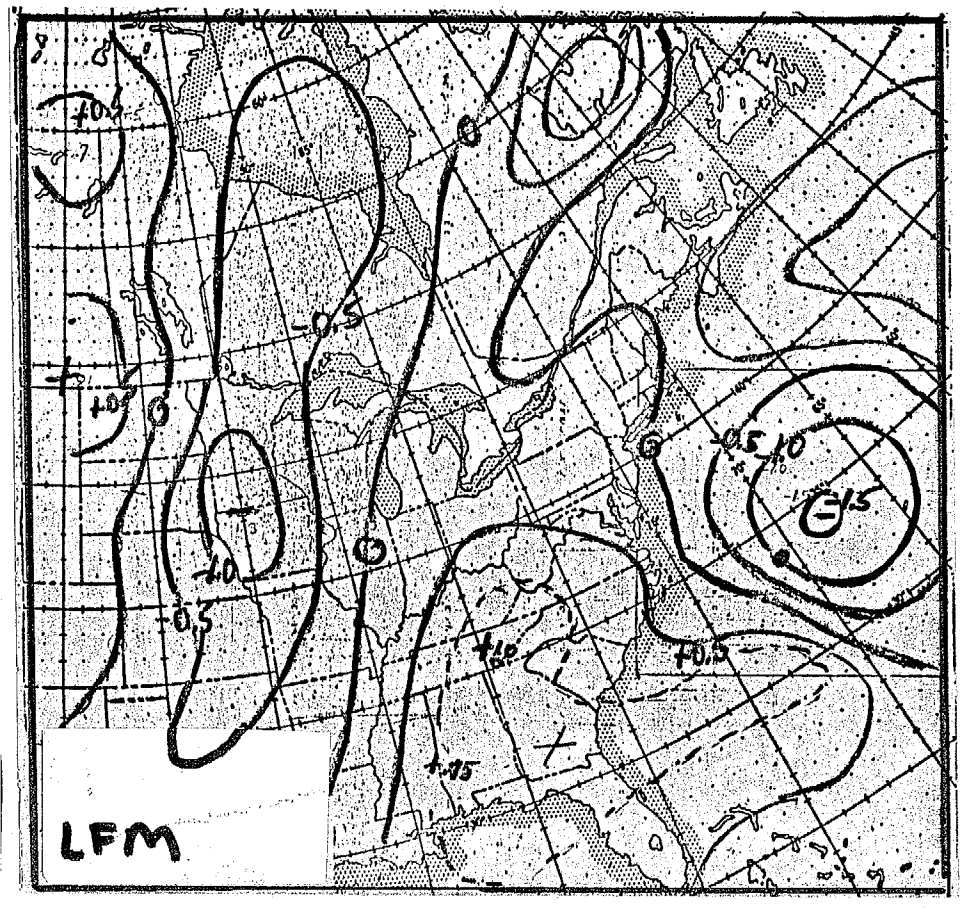

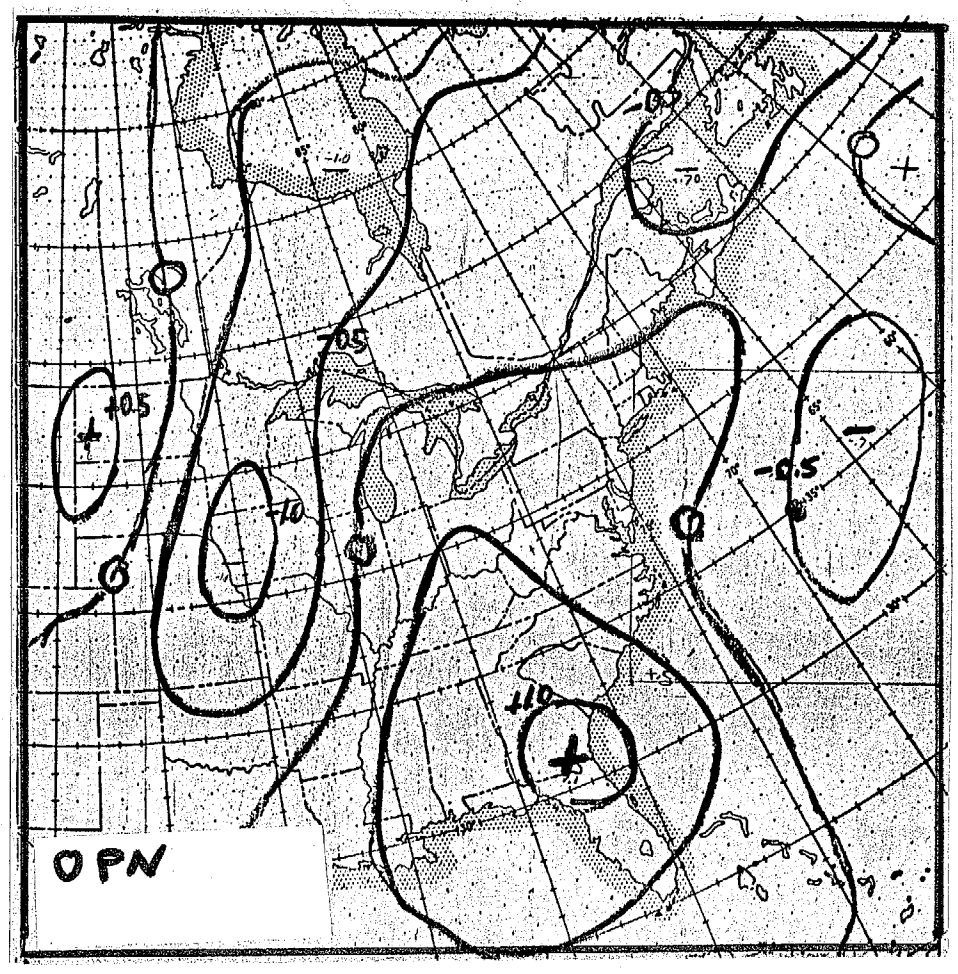

FIG 5.

LFM AND OPN TOTAL SLP TEND (mb hr⁻¹). ● => SURFACE LOW POSITION.

1200 22 FEB 1978

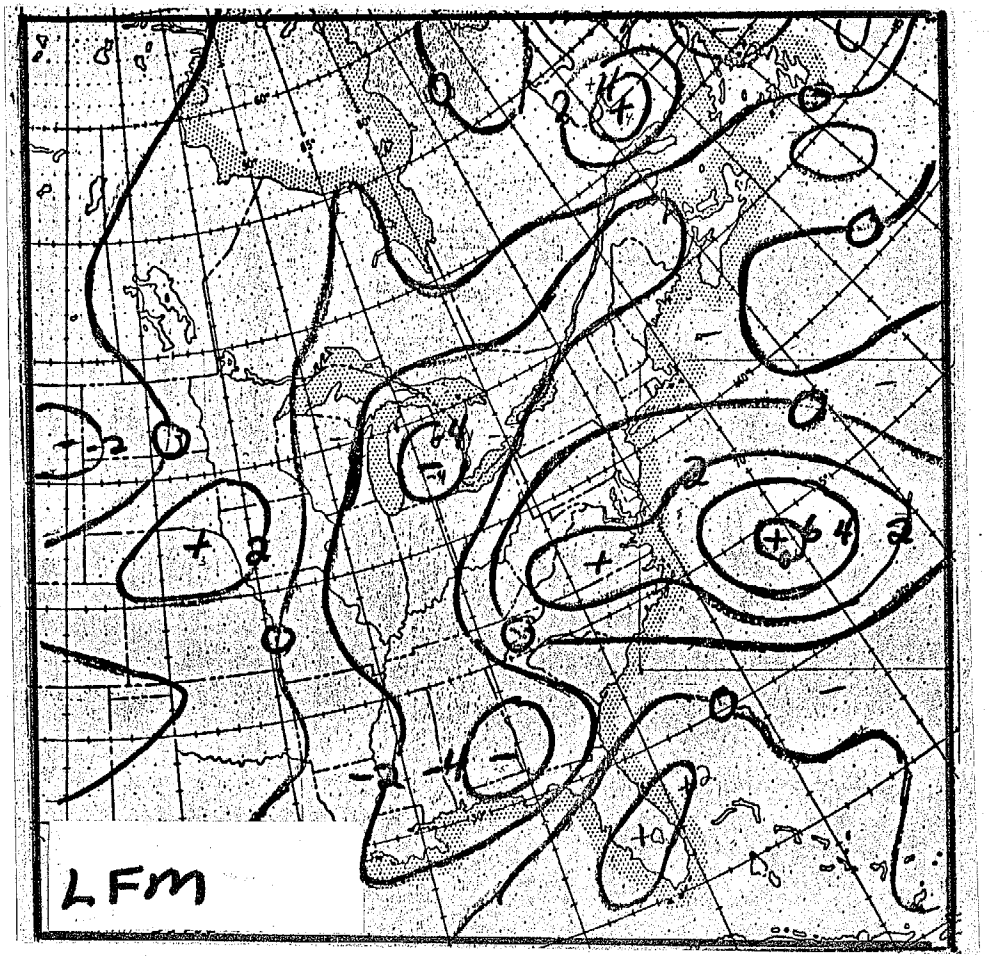

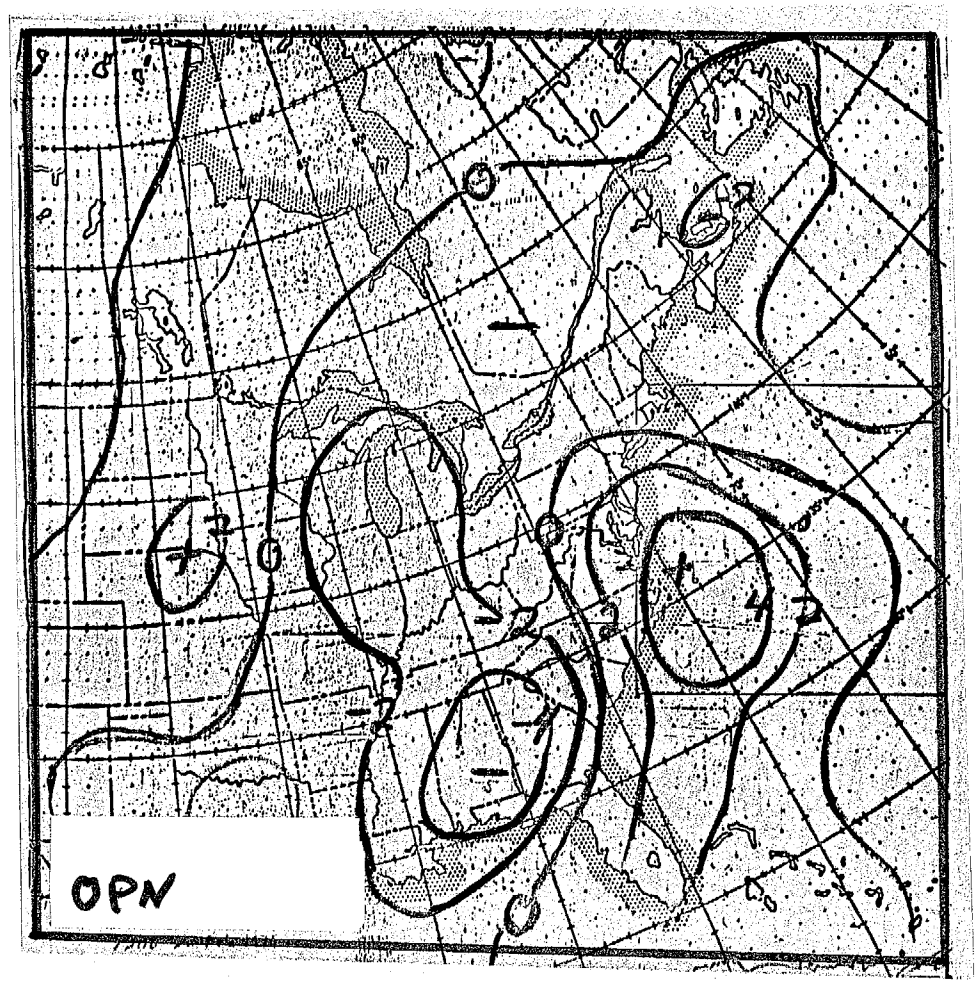

FIG. 6

LFM AND OPN VORT. ADV.
700 mb VERT. VEL (cm sec⁻¹)
1200 22 FEB 1978

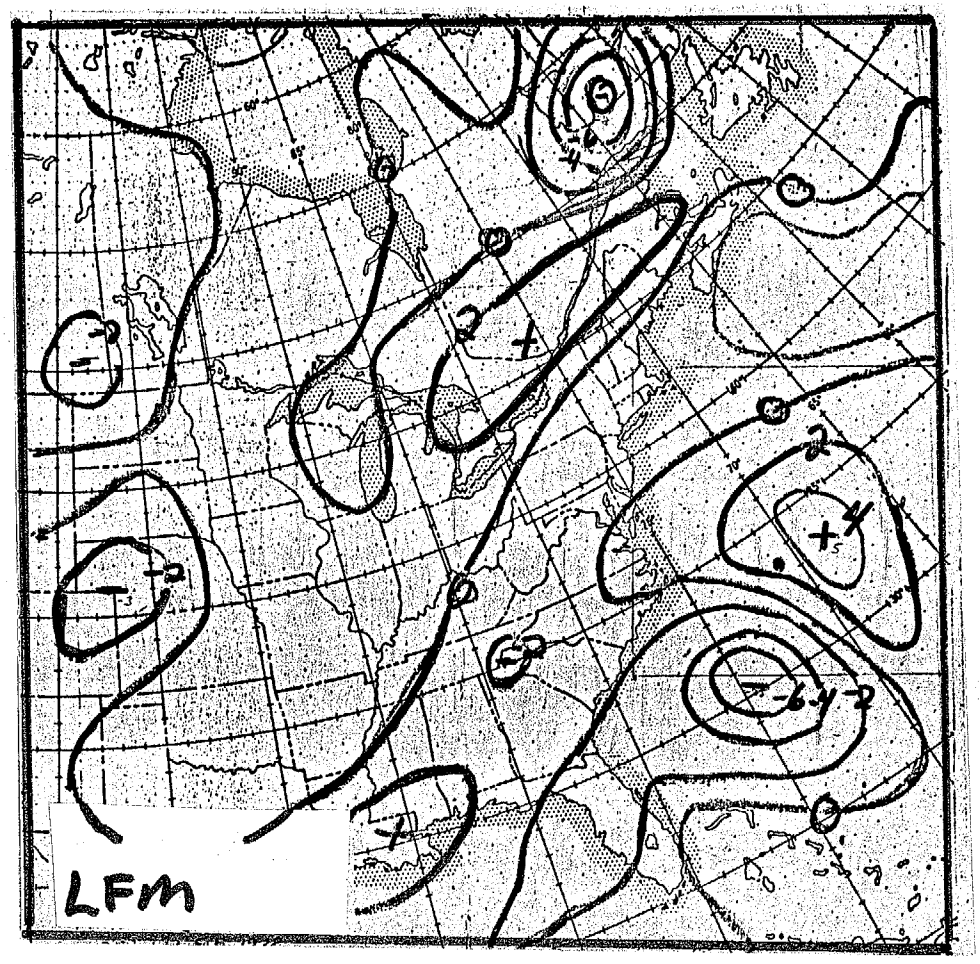

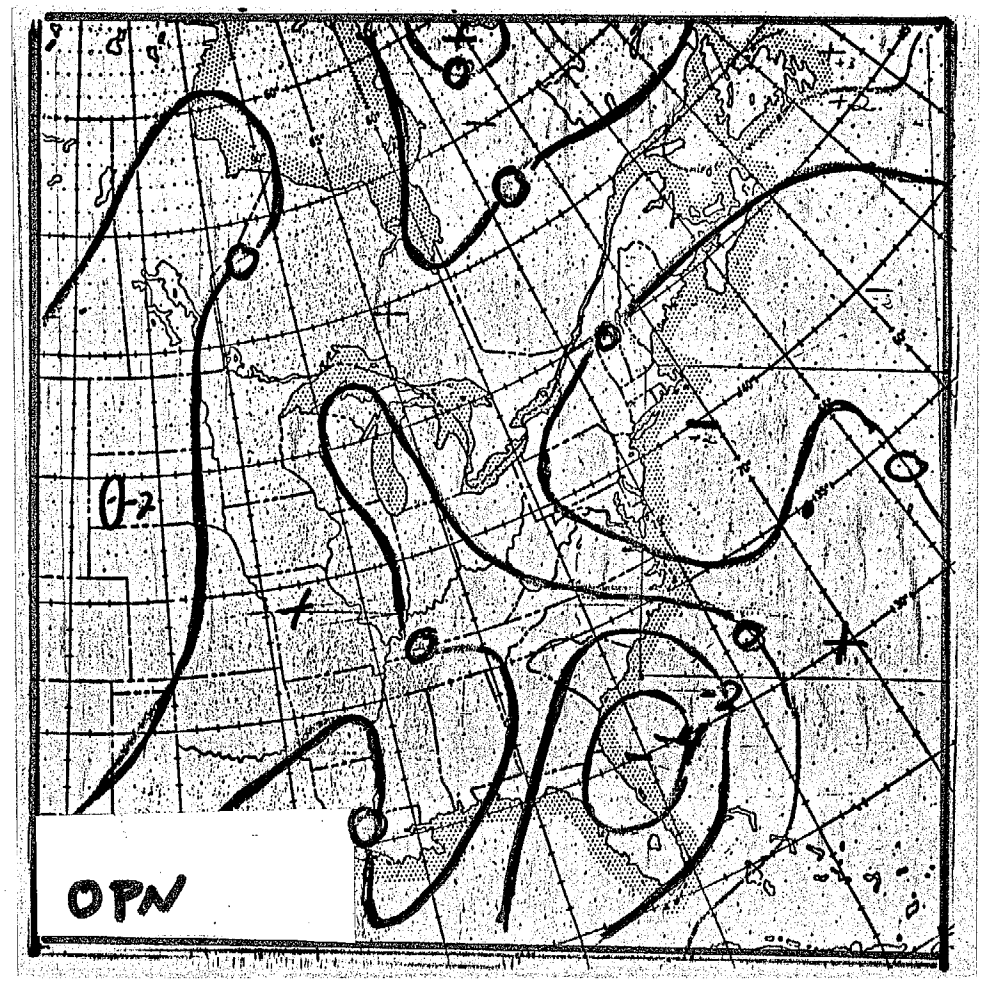

FIG 7.

LFM AND OPN THERMAL ADV. 700 mb VERT VEL (cm sec⁻¹)

1200 22 FEB 1978

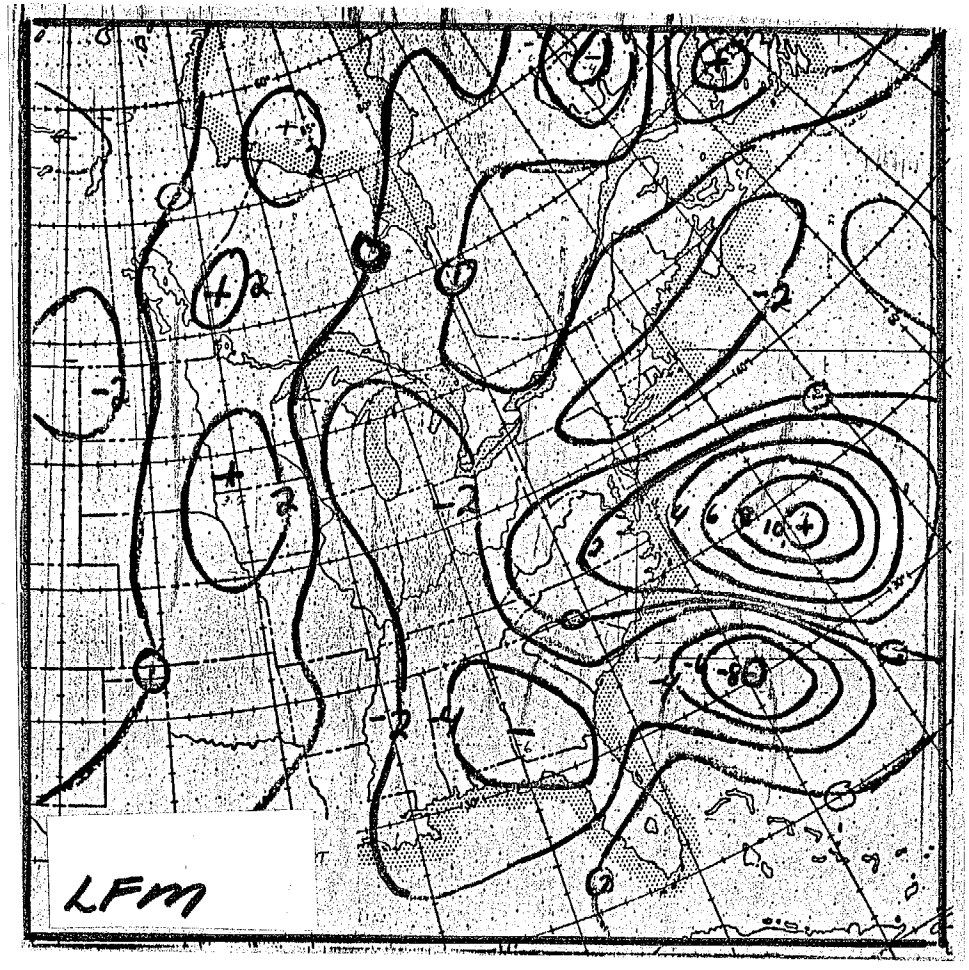

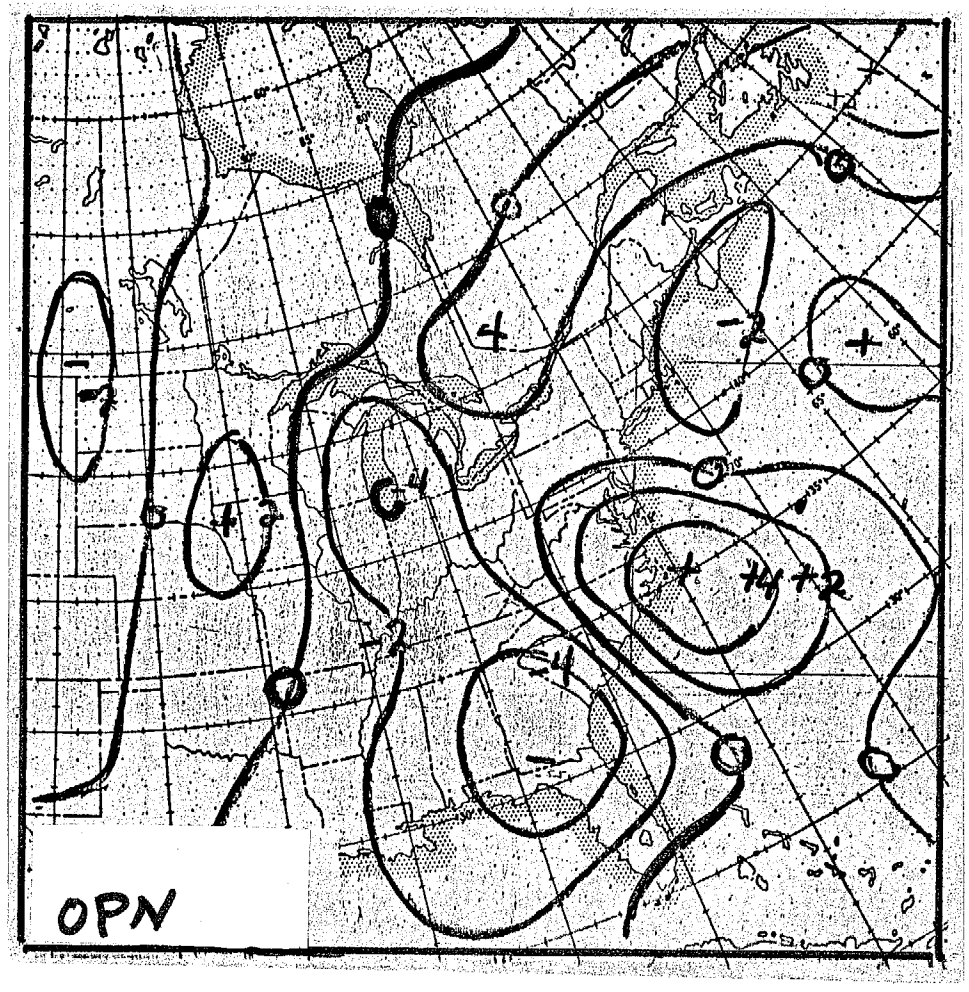

FIG. 8

LFM AND OPN TOTAL
700 mb VERT VEL (μb sec⁻¹)

1200 22 FEB 1978

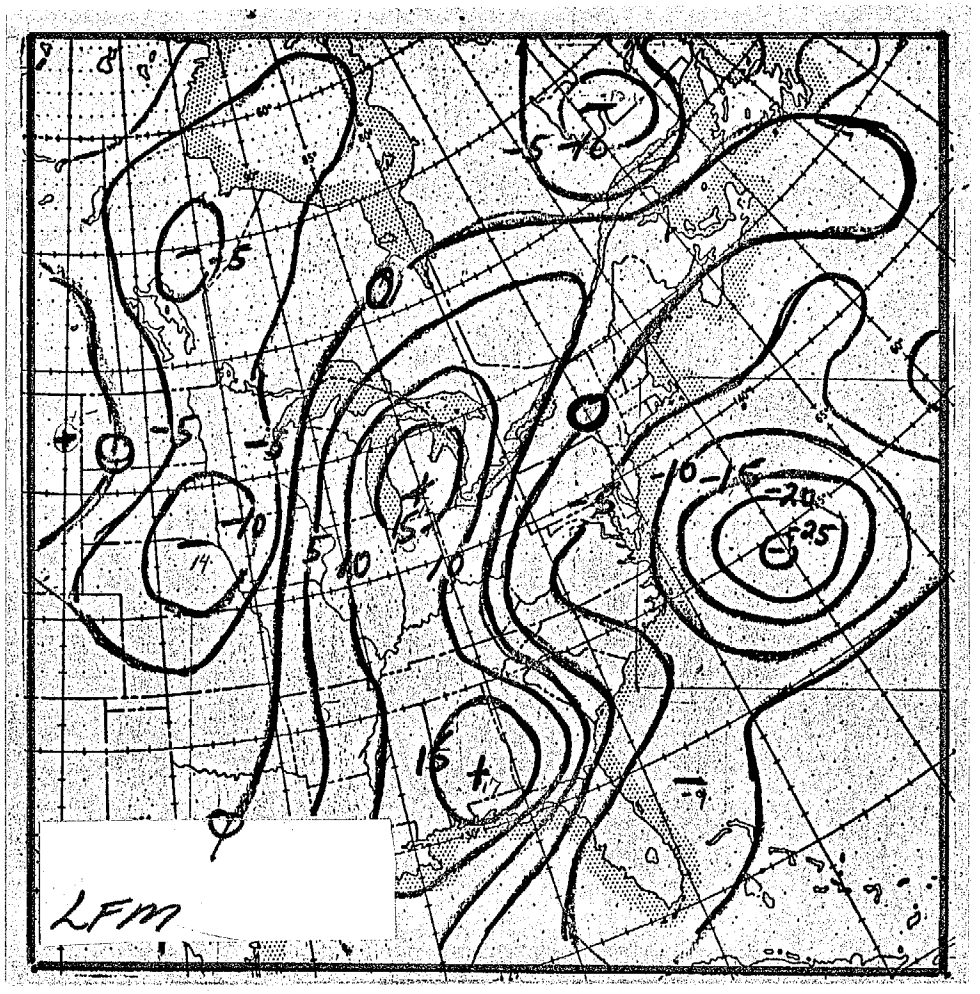

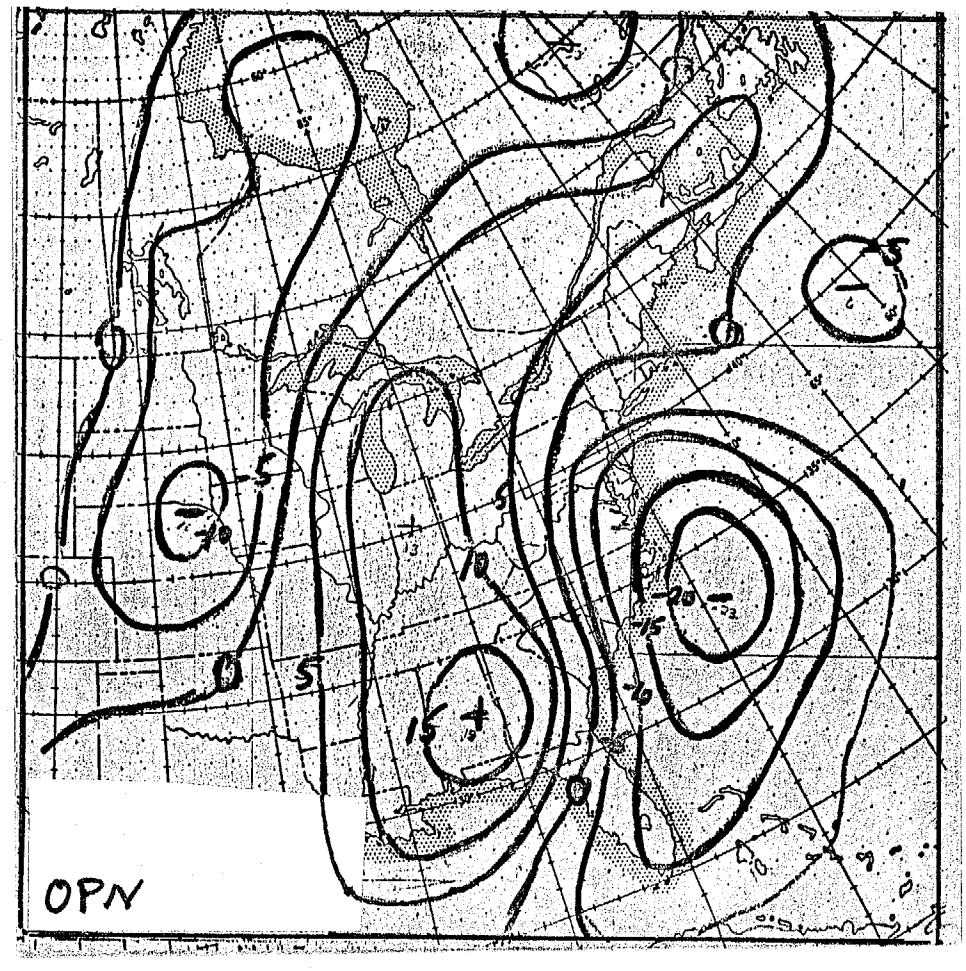

FIG 9

LFM AND OPN TOTAL 500mb ht tend (m hr⁻¹)

1200 22 FEB 1978

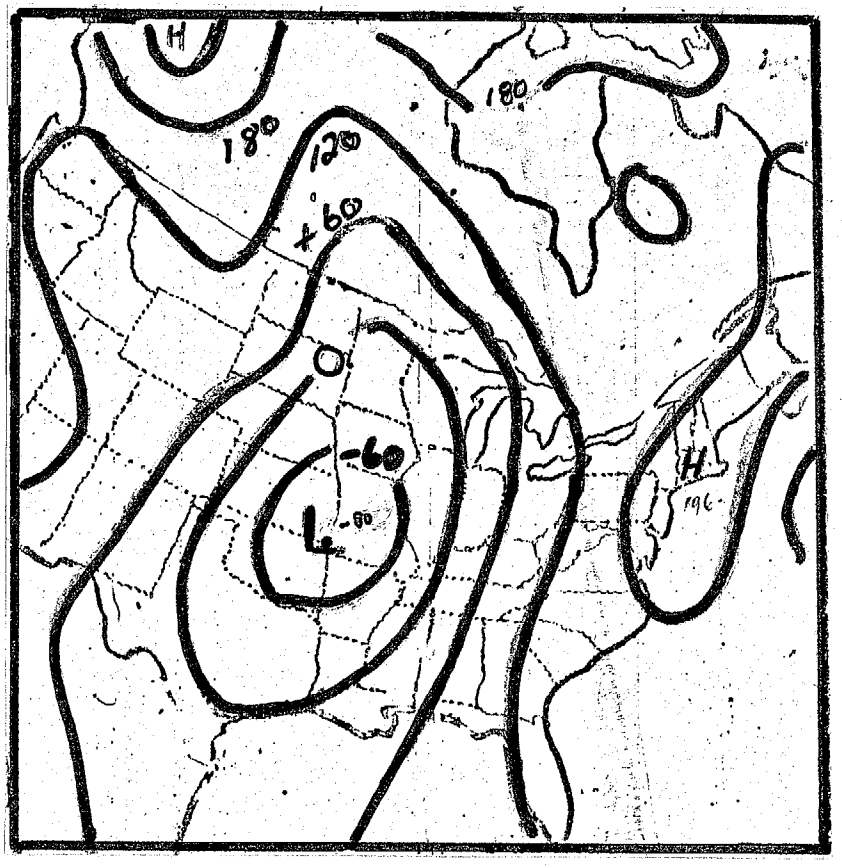

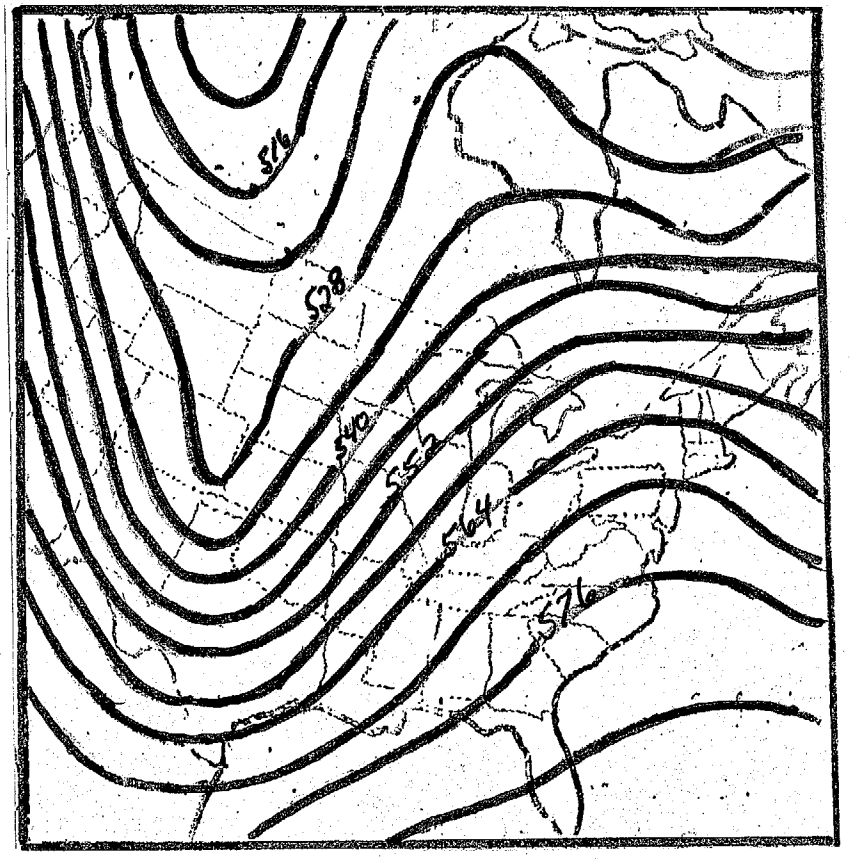

FIG. 10.
FINAL 1000 AND 500mb
ht, 1200 10 JAN 75

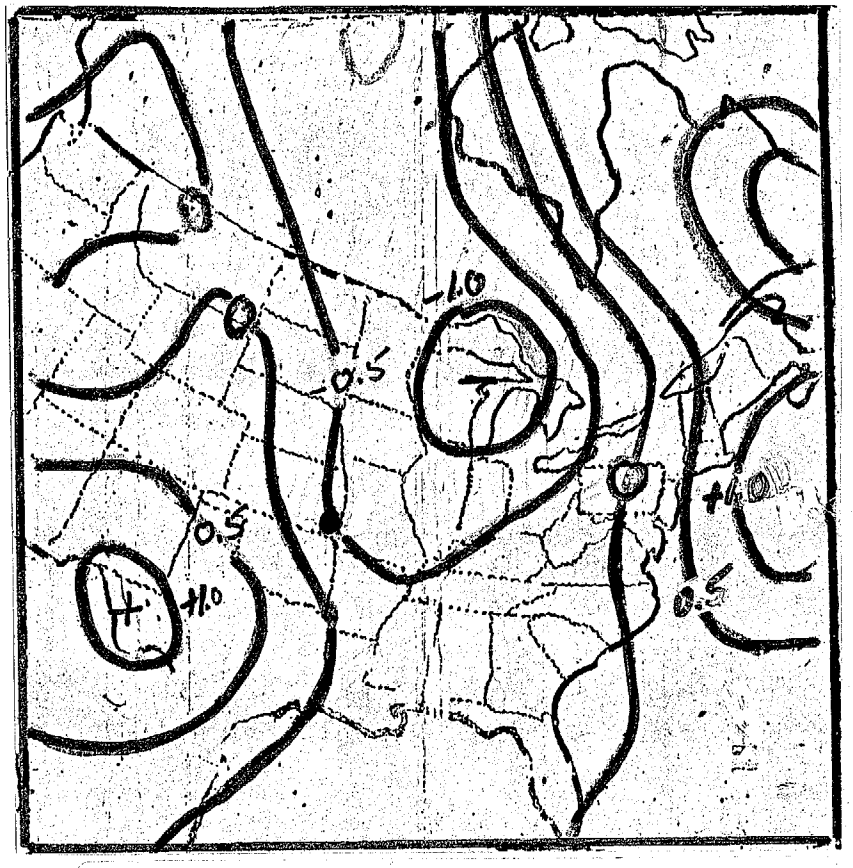

FIG. 11.
TOTAL SLP TEND (mb hr^{-1}),
1200 10 JAN 1975
(FROM FINAL ANAL)

FIG. 12.
TOTAL 500mb GEOPENTIAL
TEND. CONTOUR INTERVAL
IS 100×10^{-4} m^2 sec^{-3} ($\approx$3.7m hr^{-1})
1200 10 JAN 75
(FROM FINAL ANAL)

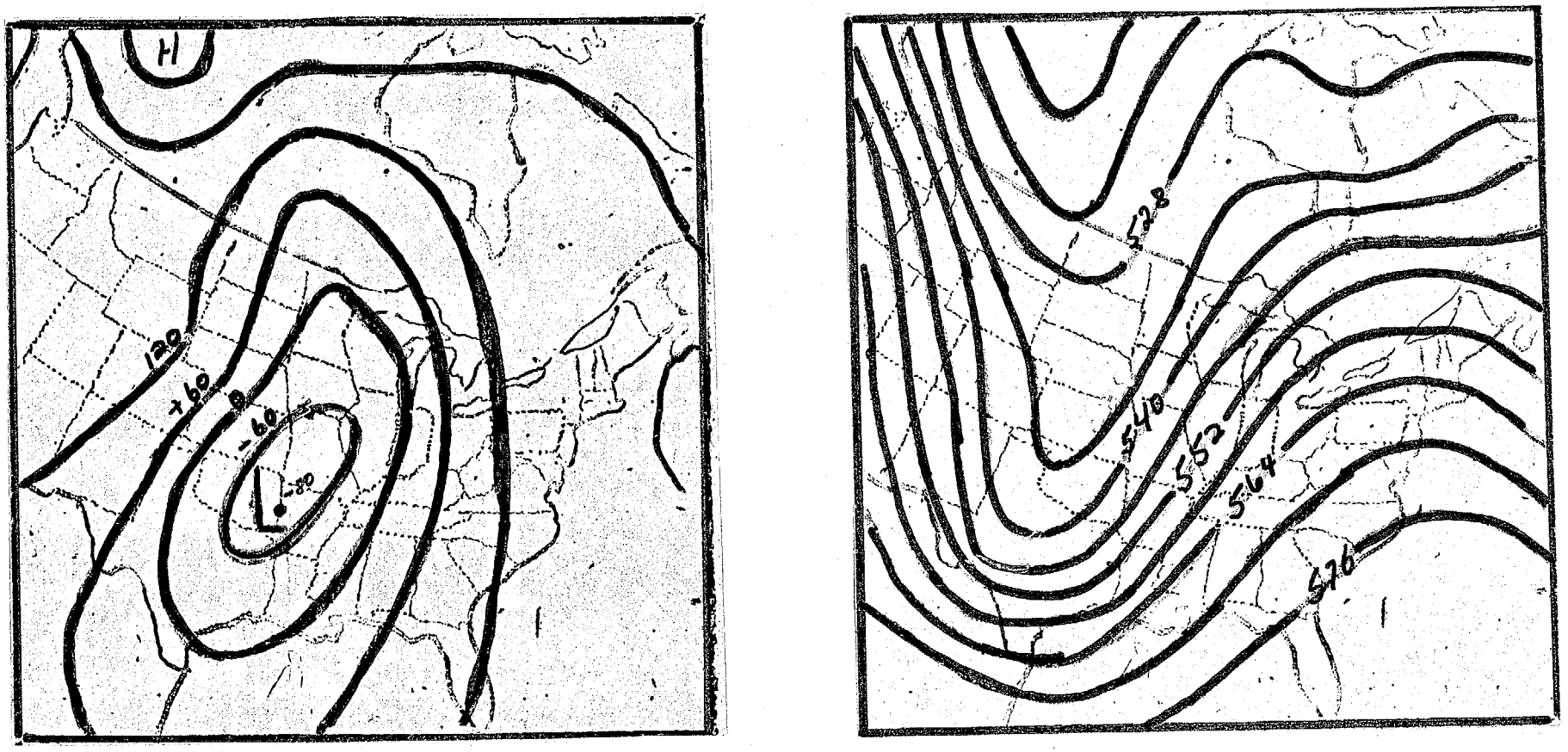

FIG. 13A.

24 hr 7-LAYER 1000 AND 500mb ht. VERIFYING 1200 10 JAN 1975

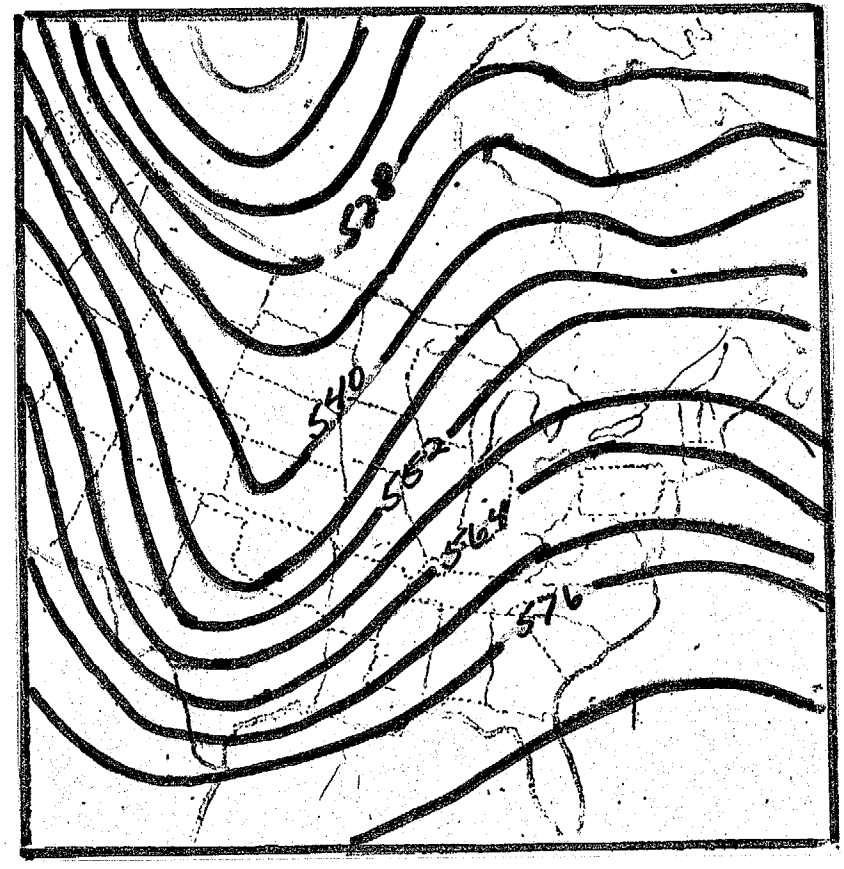

FIG 13B
24hr NGM 1000 AND
500mb ht. VERIFYING
1200 10 JAN 1975

7-LAYER

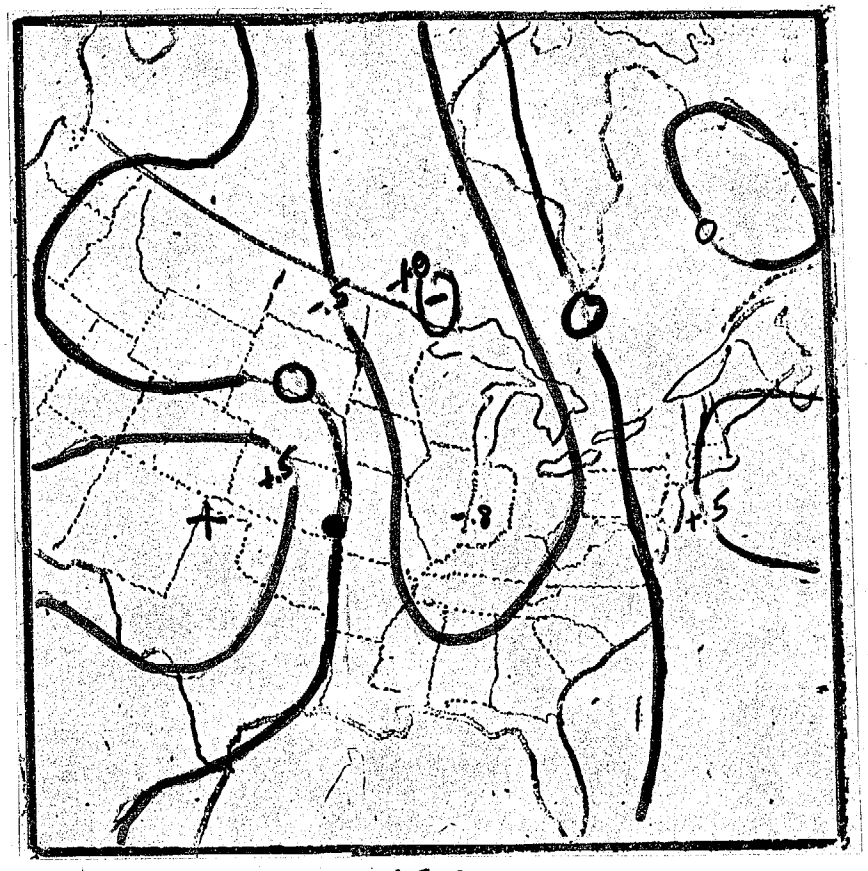

NGM

FIG 14.
24hr 7-layer AND NGM
TOTAL SLP tend (mb hr^{-1})
VERIFYING 1200 10 JAN 1975

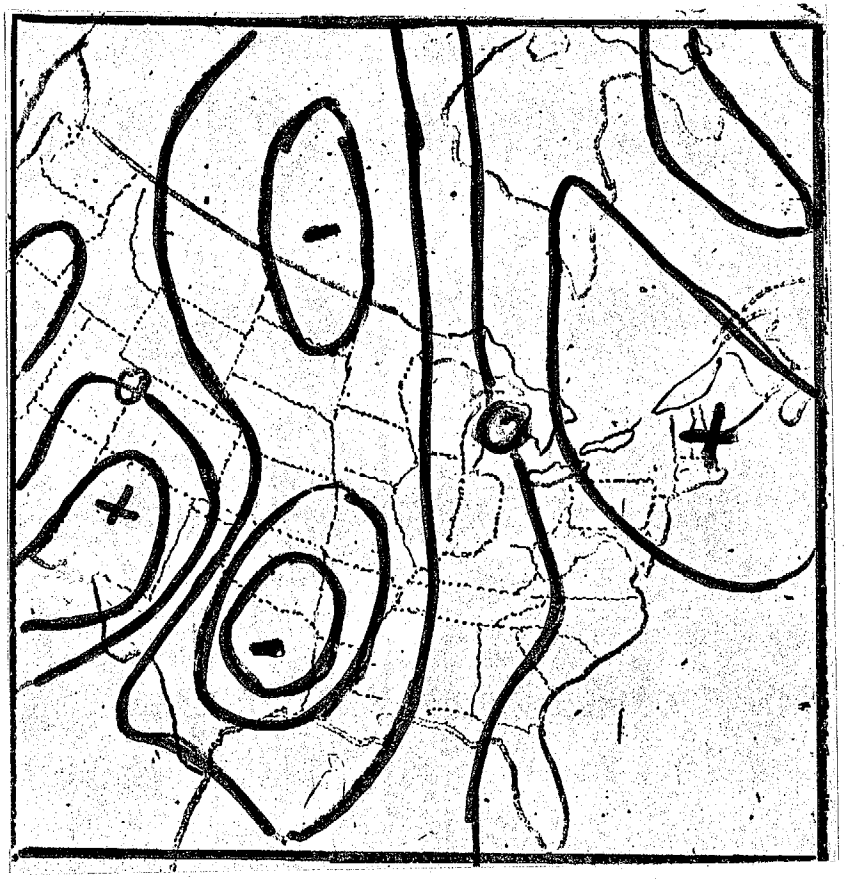

7-LAYER

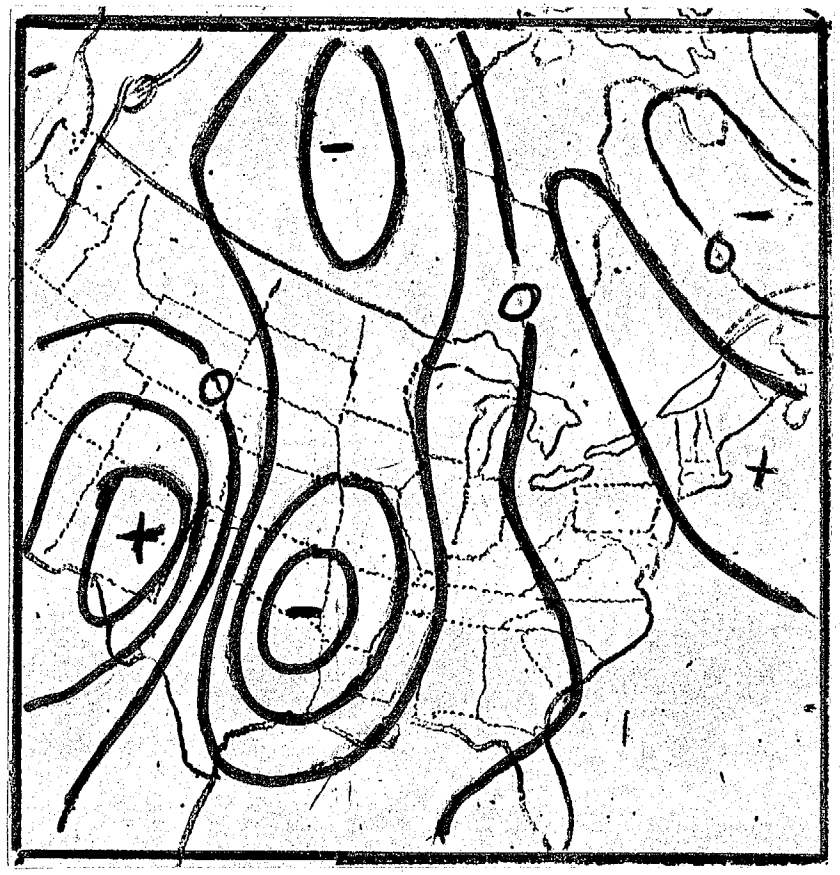

NGM

FIG 15.
24 hr 7-layer AND NGM
TOTAL 500mb GEOPOTENTIAL
TEND. CONTOUR INTERVAL,
SAME AS FIG 12.
VERIFYING 1200 10 JAN 1975

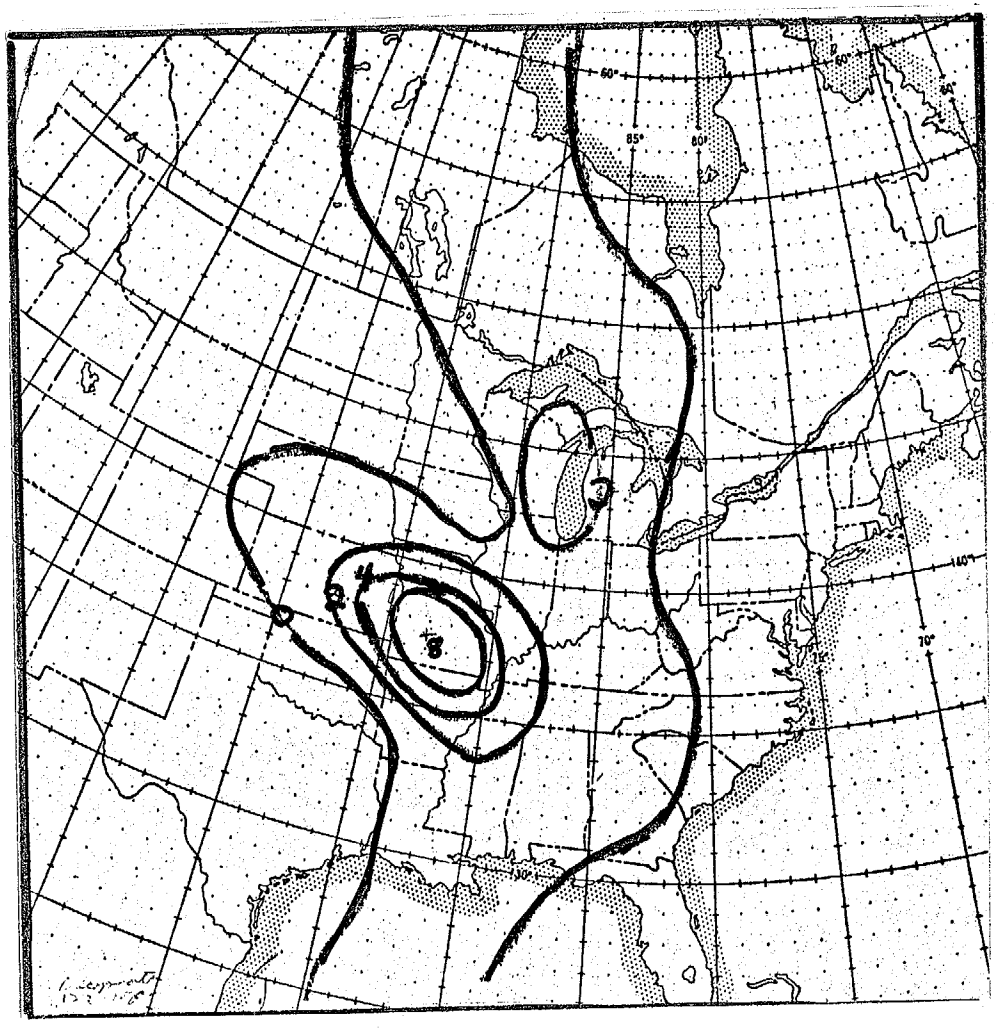

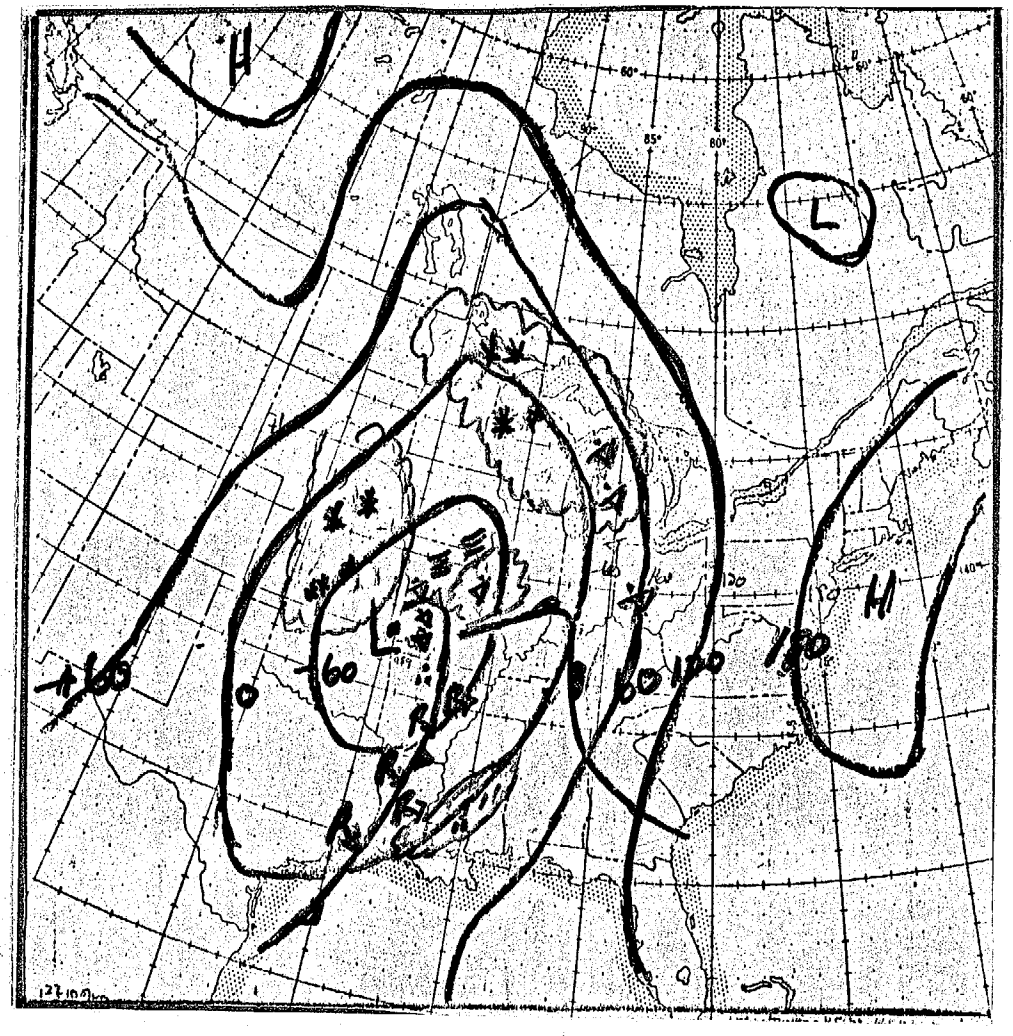

FIG. 16
DIAGNOSTIC PRECIP RATE (hundreths hr^{-1}), AND 1000 mb ANAL WITH SURFACE FRONTS AND WEATHER
1200 10 JAN 1975

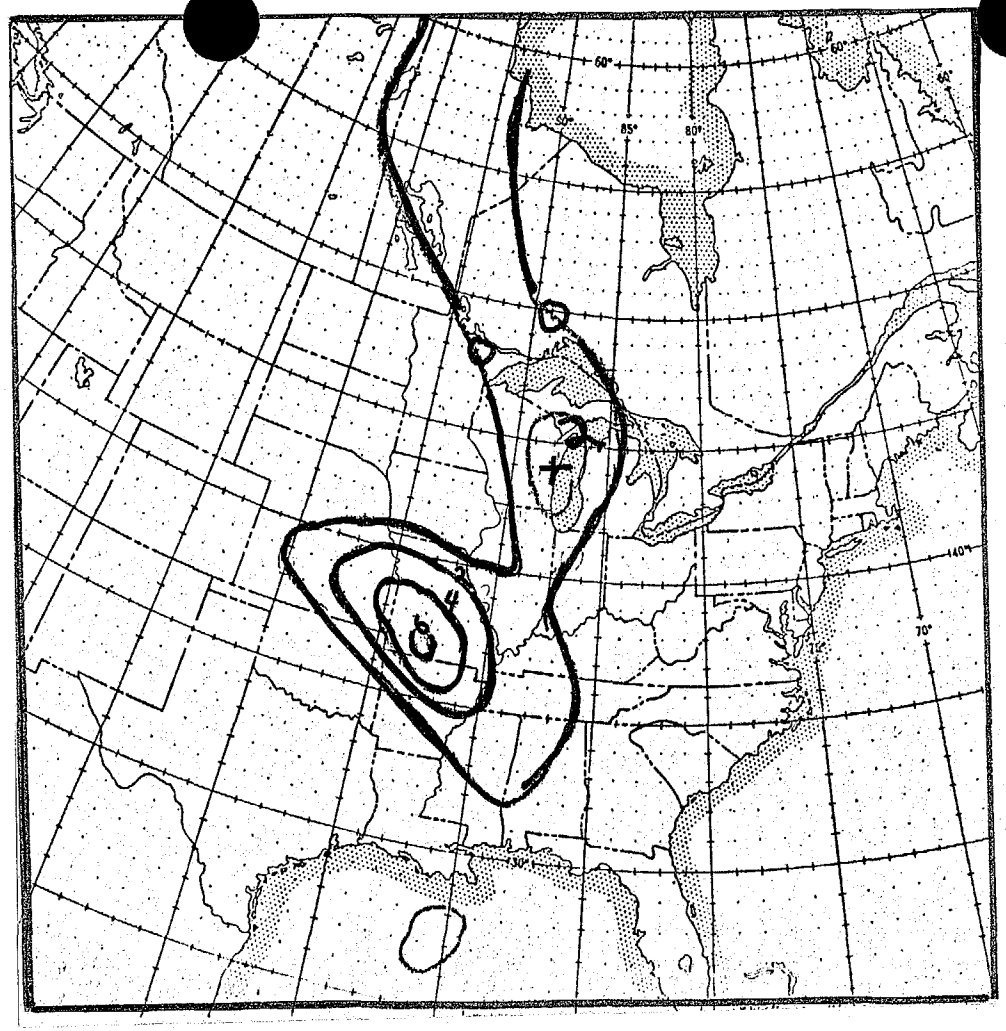

FIG 17.
LATENT HEAT 700 mb VERT. VEL (cm sec^{-1})
1200 10 JAN 1975

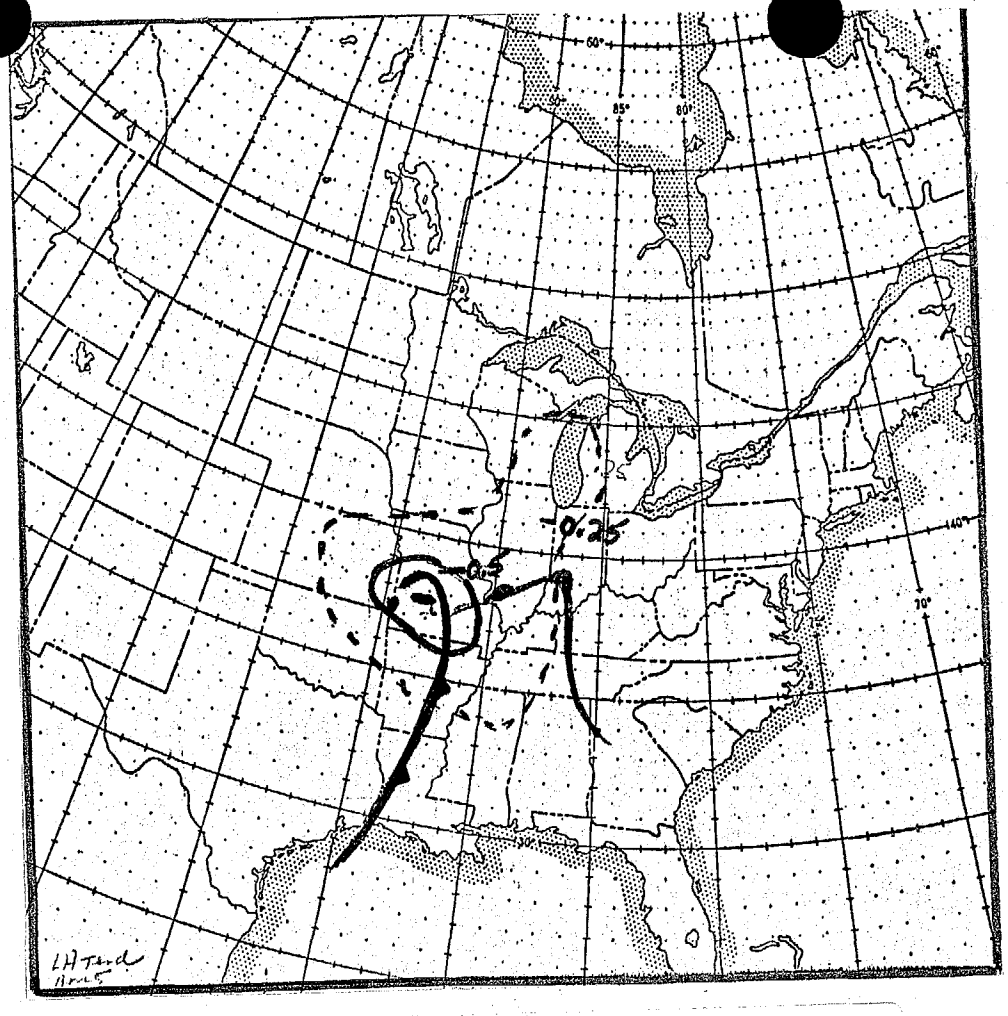

FIG 18.
LATENT HEAT SLP TEND. (mb hr^{-1})
1200 10 JAN 1975

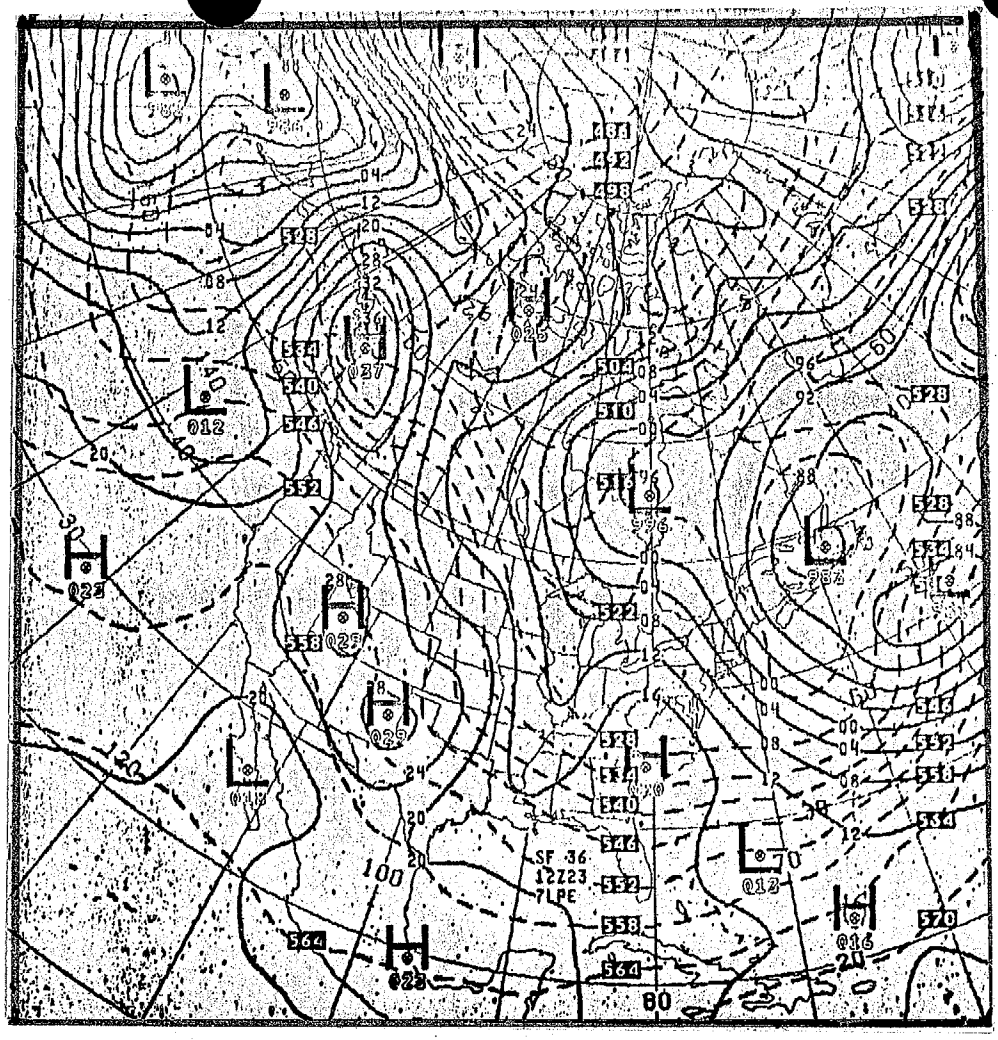

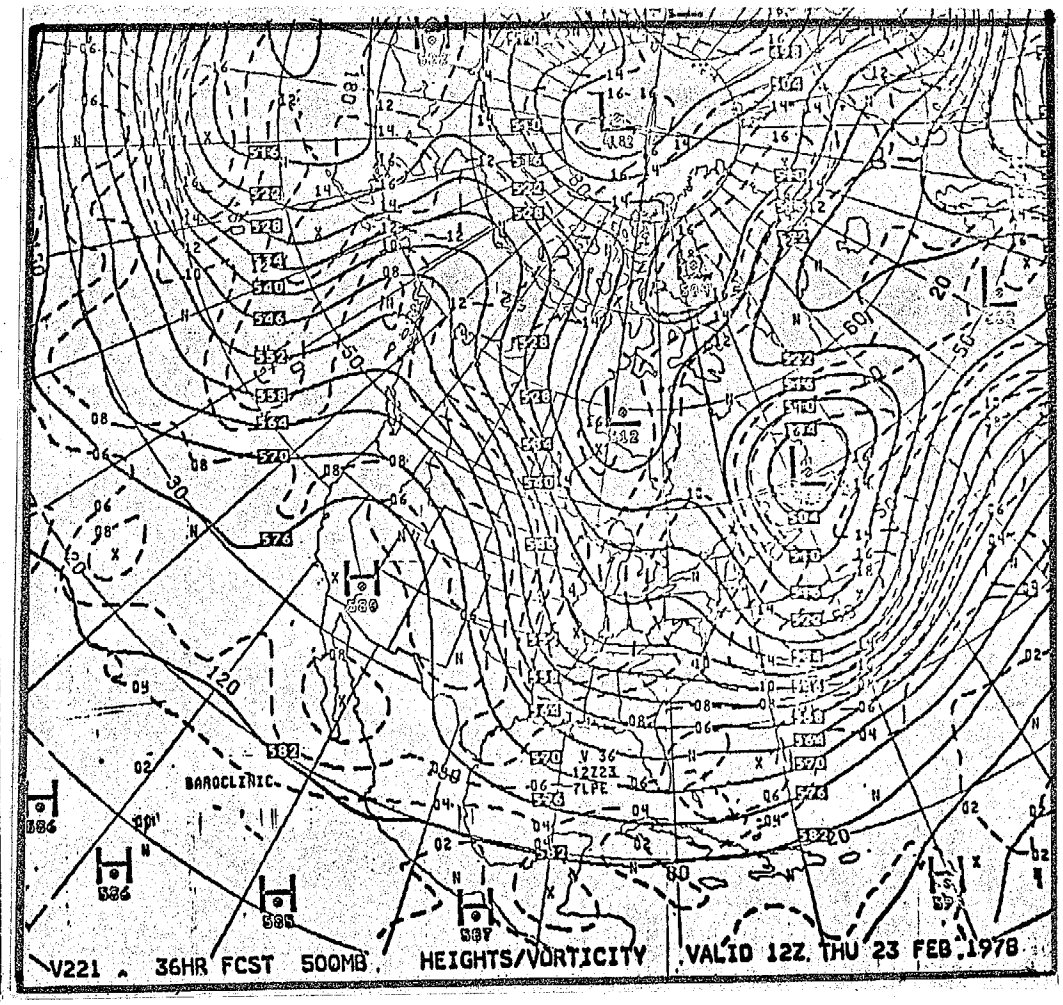

FIG 19

36 hr 7-layer surface/thick.

and 500mb ht/vort. valid

1200 23 Feb 1978

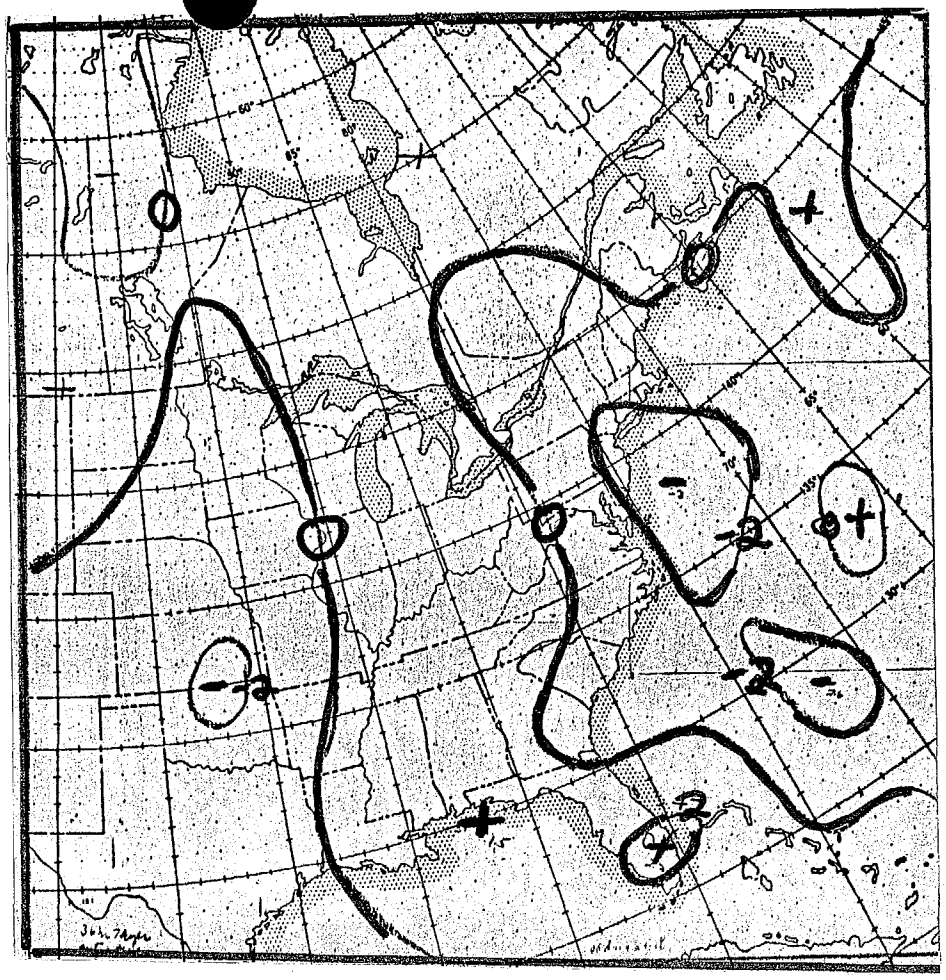

FIG. 20.
36 hr 7-layer 700mb
Vert vel. (cm sec⁻¹) VALID
1200 23 Feb 78

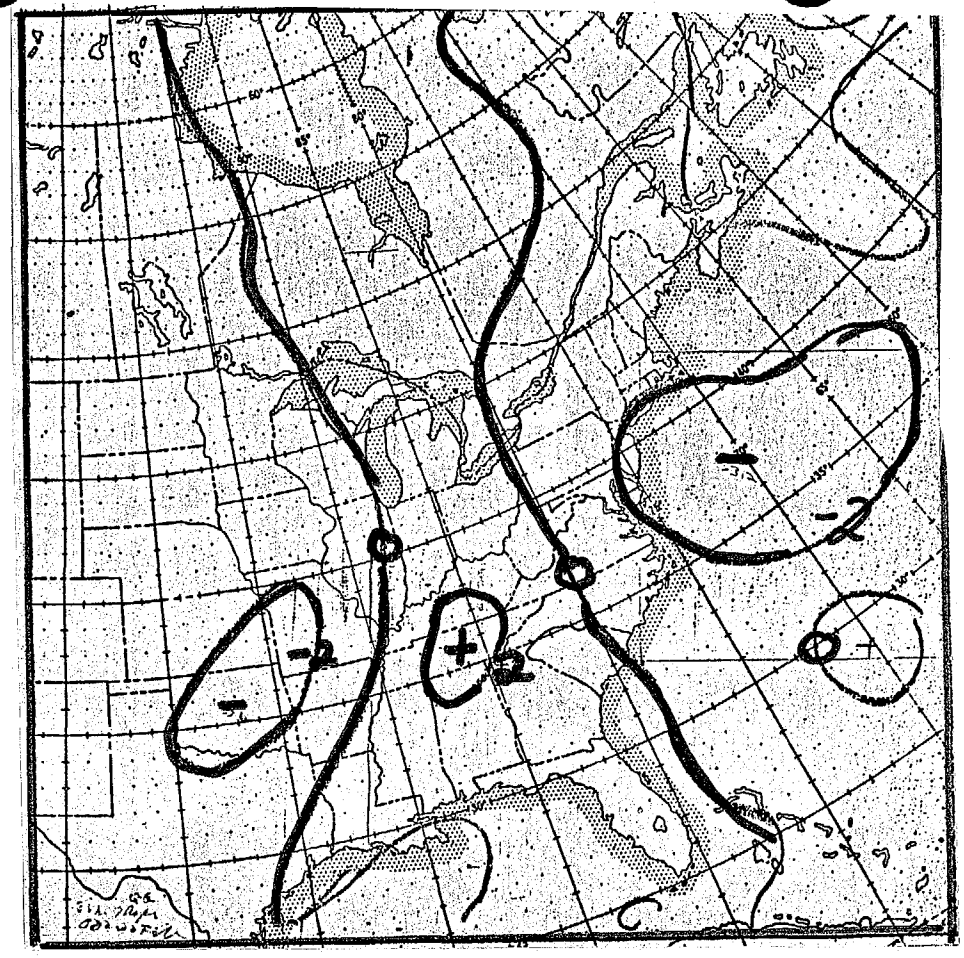

FIG 21.
36 hr 7-layer Quasi-Geos.
700mb vert vel (cm sec⁻¹)
VALID 1200 23 FEB 78

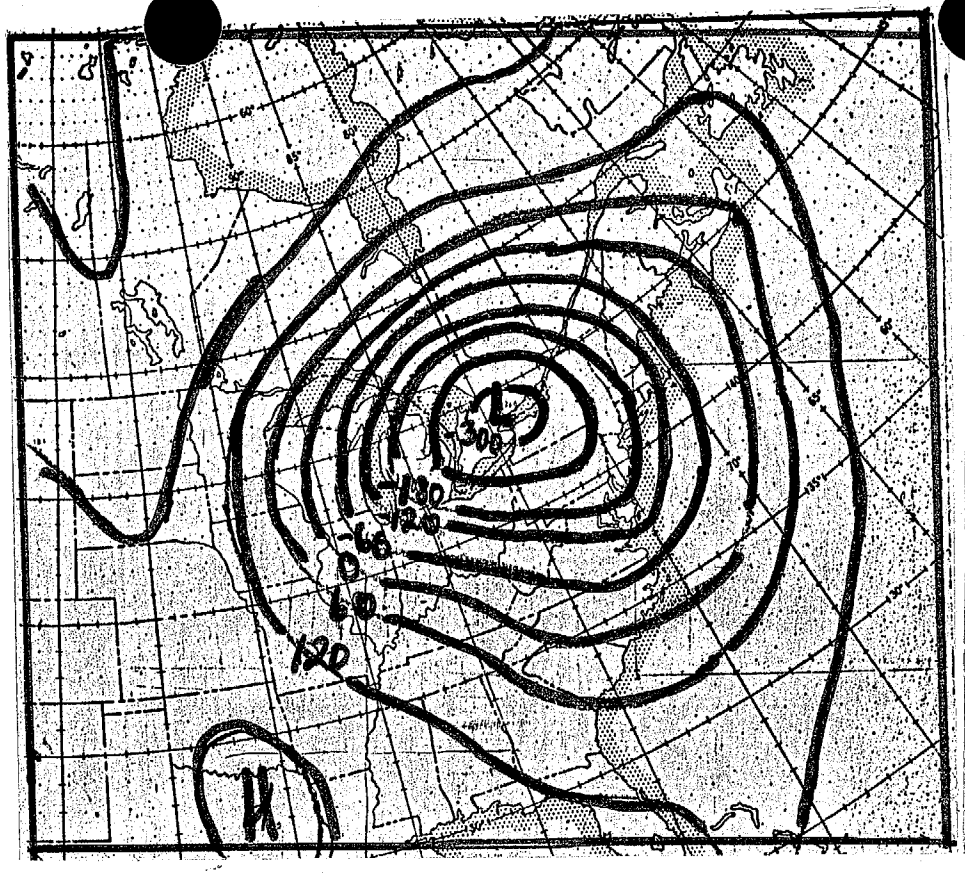

LFM

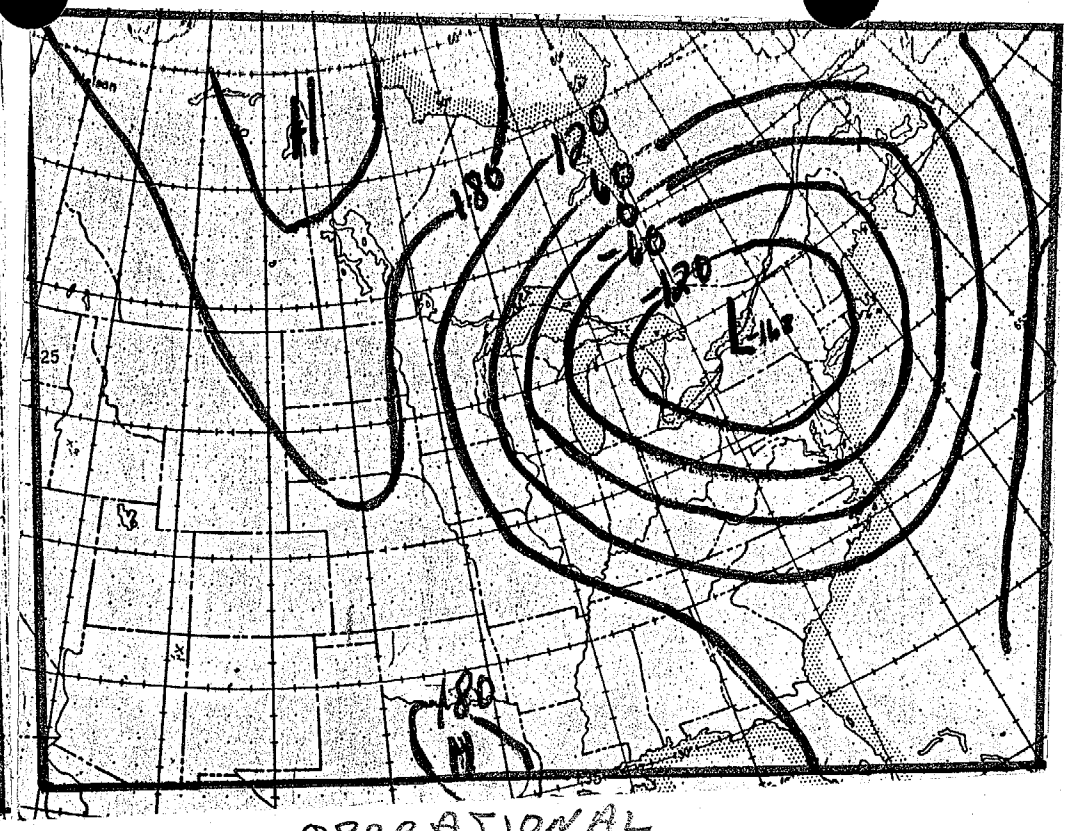

OPERATIONAL

FIG 22

LFM AND OPERATIONAL

1000 mb ht, 1200 26 JAN 78

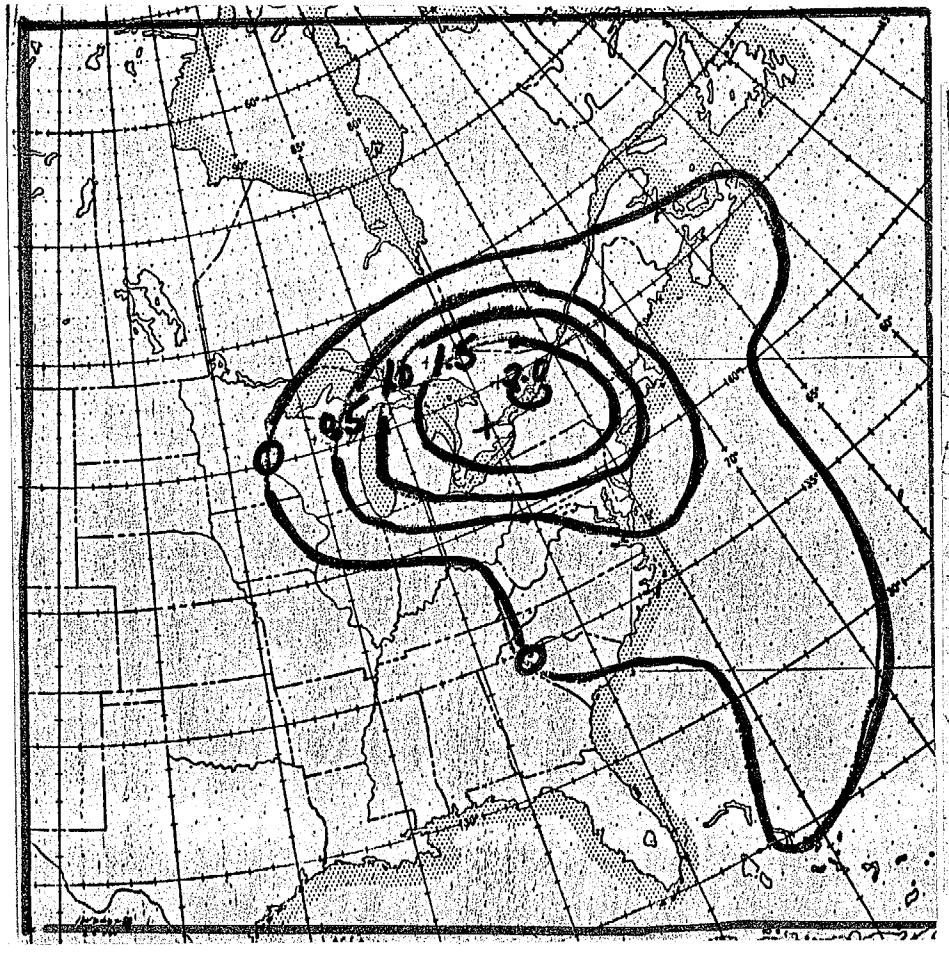

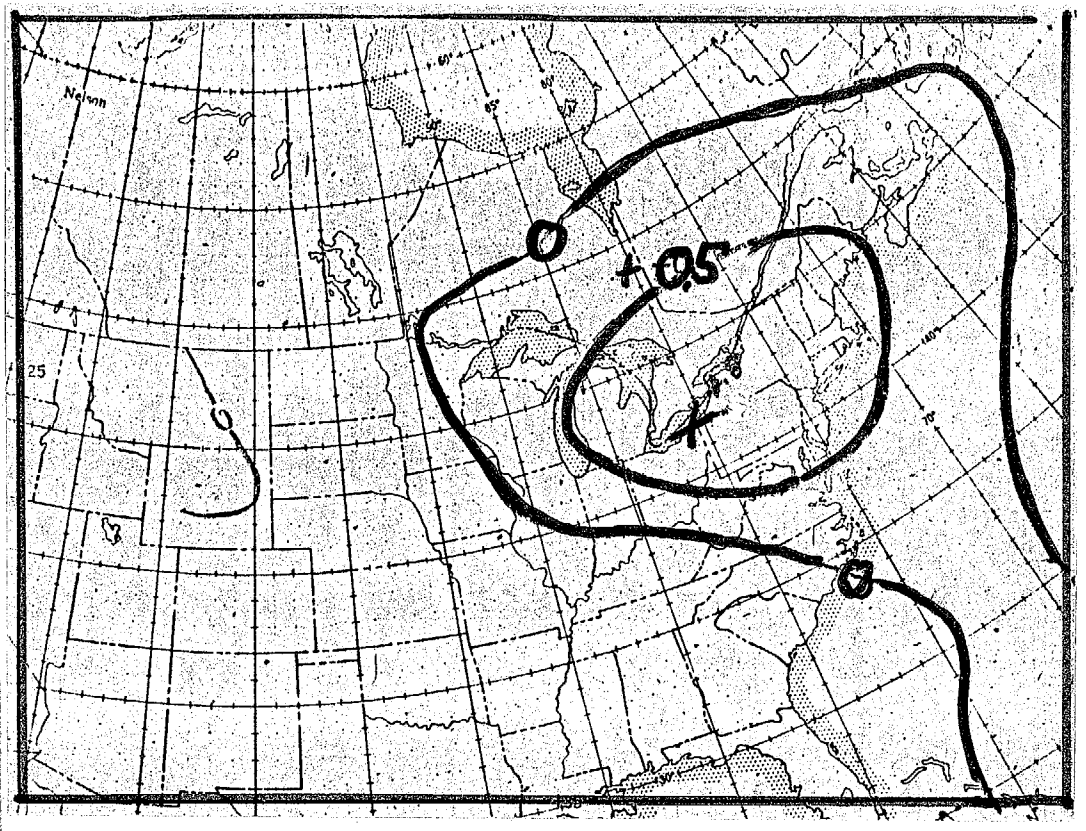

FIG. 23

LFM AND OPERATIONAL FRICTION SLP tend (mb hr⁻¹)

1200 26 JAN 78